Enhanced Desorption in Novel Sorbent Materials Using Ultrasound

by

Weston K. Bertrand

A Thesis Presented in Partial Fulfillment
of the Requirements for the Degree
Master of Science

Approved April 2018 by the
Graduate Supervisory Committee:

Patrick Phelan, Chair
Liping Wang
Luis Bocanegra
Shankar Devasenathipathy

ARIZONA STATE UNIVERSITY

May 2018

ABSTRACT

In this study, two novel sorbents (zeolite 4A and sodium polyacrylate) are tested to investigate if utilizing ultrasonic acoustic energy could decrease the amount of time and overall energy required to regenerate these materials for use in cooling applications. To do this, an experiment was designed employing a cartridge heater and a piezoelectric element to be simultaneously providing heat and acoustic power to a custom designed desorption bed while measuring the bed mass and sorbent temperature at various locations. The results prove to be promising showing that early in the desorption process ultrasound may expedite the desorption process in zeolite by as much as five times and in sodium polyacrylate as much as three times in comparison to providing heat alone. The results also show that in zeolite desorption utilizing ultrasound may be particularly beneficial to initiate desorption whereas in sodium polyacrylate ultrasound appears most promising in the after a temperature threshold is met. These are exciting results and may prove to be significant in the future as more novel heat-based cooling cycles are developed.

ACKNOWLEDGMENTS

I would like to thank my advisor, Prof. Patrick Phelan for advice and guidance as I have been working in his lab these last few years. I am very grateful for the opportunities he helped me pursue. I would also like to thank the other members of my committee, Prof. Luis Bocanegra, Prof. Liping Wang, and Dr. Shankar Devasenathipathy for their help in the work resulting in this thesis. Each of them has gone out of their way to ensure I have the information and tools I need to succeed and that is very much appreciated. I would like to recognize my supportive labmates Hooman Mobarakeh, Nico Cambell, Ahmad Bamasag, Nick Fette, Andrey Gunawan, and especially Sami M.A. Al-elyani for his infinite patience in helping me and his great friendship. Finally, I would like to thank my wonderful family for helping me through my graduate school, in particular my wife, Rachel.

TABLE OF CONTENTS

CHAPTER Page

LIST OF TABLES

Table Page

LIST OF FIGURES

Figure Page

Figure Page

Chapter 1

INTRODUCTION

In recent years, there has been a concerted effort to develop heat based cooling cycles. This effort is born of the relatively recent acceptance of man-made climate change in conjunction with a deeper understanding of the environmental and health hazards associated with currently used vapor compression cycles, the dominant refrigeration method in the global market. Furthermore, considering the currently underutilized low-grade waste heat as an energy resource provided by a host of different applications offers a very enticing alternative to electricity which may come from a source that is not environmentally friendly, such as fossil fuel driven power plant.

Adsorption refrigeration is a phenomenon that occurs when a refrigerant extracts heat from the ambient which causes it to evaporate and then be captured by an adsorbent which retains the molecules using adhesion forces. To repeat the heat extraction cycle, the gas molecules must then be removed and recondensed from the adsorbent by some energetic means. One of the critical design considerations of a adsorption refrigeration cycle is the ability of the sorbent material to both adsorb and desorb a refrigerant. Both the amount of time and energy required to absorb or desorb the refrigerant into the sorbent material are of primary concern. Thus, materials that are able to adsorb large amounts of refrigerant (relative to their dry mass) and desorb with low energy input are of particular interest in this field. Given the recent focus on adsorption cooling, materials that have previously not been considered for refrigeration applications are now being investigated as novel sorbents. Two such examples of such materials is are zeolite 4A and sodium polyacrylate. Additionally, novel ways to reduce the overall energy required to regenerate sorbents is of interest

in the field of heat driven cooling such as leveraging ultrasonic acoustic energy to aid in the desorption process.

1.1 Using Zeolite as an Adsobent

Zeolites (also called molecular sieves) are microporous aluminosilicate minerals that were first discovered in nature in 1756 and first atificially synthesized in the 1940s [1]. Since then, zeolites have been purposed for a variety of applications, most common of which are chemical catalysis, ion exchange, and adsorption (also called gas separation)[2]. This last application has recently been of interest for use in adsorption cooling given zeolites' ability to adsorb various refrigerants through its micropores. By using these tiny pores (to the order of three to ten angstroms), gas molecules can be captured and retained through the adhesion forces from inside the pore. A visual representation of the chemical structure of zeolite which is responsible for these micropores and a microscopic view of the physical structure are shown in Figures 1.1 [3] and 1.2 [4] .

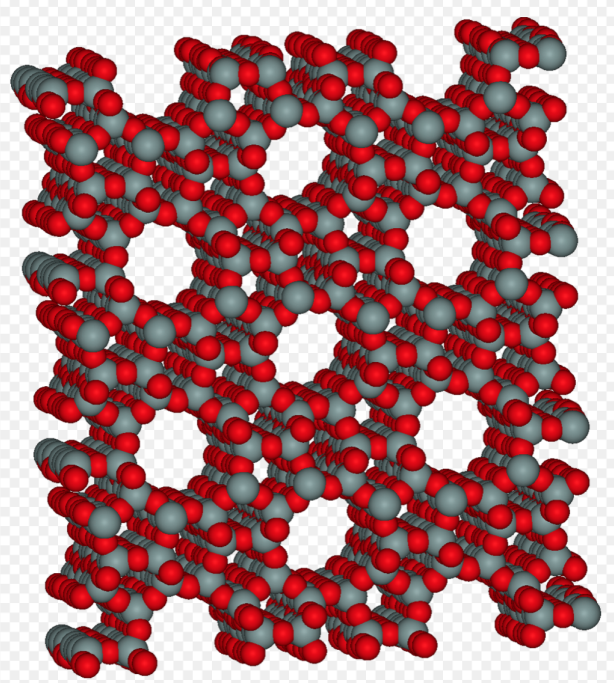

Figure 1.1: Chemical Structure of Zeolite [3]

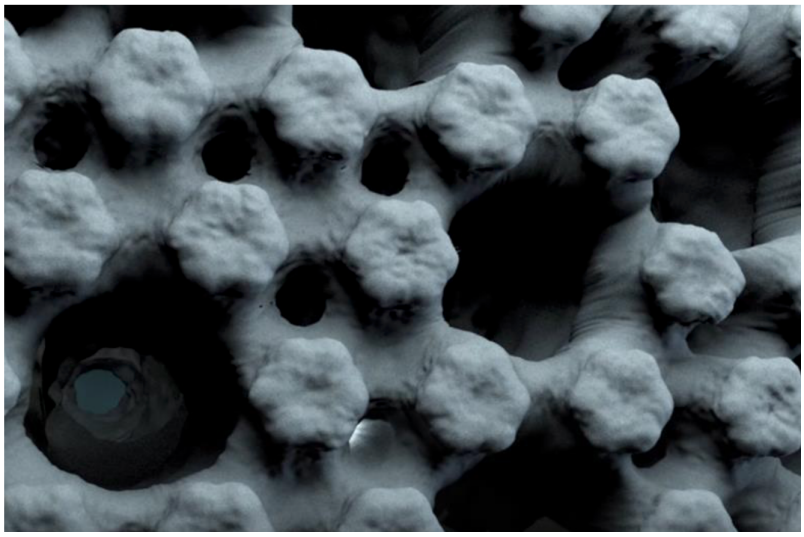

Figure 1.2: Microscopic View of Zeolite Sample [4]

The pore size and shape dictate what kind of gases can be captured (depending on molecule size), how much gas can be captured, and the amount of energy is required

to overcome the adhesive forces and release the gas molecules. For the application of adsorption cooling, that last property is particularly important since the amount of energy required to remove the gas molecules will determine how efficiently cooling can be produced.

1.2 Ultrasound Generation Using a Piezoelectric Element

Ultrasound is defined as sound waves that have a frequency greater than what the human ear is capable of hearing (greater than 20kHz) [5]. Ferroelectric ceramics (also called piezoelectrics) can generate ultrasound by taking advantage of the phenomenon known as piezoelectricity which stipulates that when ferroelectric ceramics are subject to an electric field the polarization of the crystal structure can generate mechanical strain which correspondingly can generate ultrasound. This process can occur in reverse, as well (if a piezoelectric is subject to mechanical strain the crystal structure will generate an electric field) and these materials are used for a wide range of applications from musical instruments to humidifiers. This behavior is characterized by a set of coupled governing equations, in terms of the tensor quantites of the magnitude of stress and strain (T_{ij} and S_{ij}) and the vector quantites of the magnitude of the electric field and dielectric displacement (E_i and D_i), shown below [5].

$$S_{ij} = s^{E_i} T_{ij} + d_t E_i \tag{1.1}$$

$$D_i = dT_{ij} + \epsilon^{T_{ij}} E_i \tag{1.2}$$

Where s^E is the matrix of elastic compliance, d is the matrix of piezoelectric charge coefficients, d_t is the transpose of d, and ϵ^T is the permittivity matrix. This characterized relationship between mechanical and electrical conditions is determined by the material properties of the piezoelectric element and are generally considered constant at set mechanical/electrical conditions.

1.3 Sodium Polyacrylate, a Superabsorbent Polymer

Zeolite is considered one of the classic sorbent materials used in adsorbent cooling cycles and there have been numerous studies evaluating its performance in that application, though none of them have been in conjunction with ultrasonic enhancement. However, while performing this study there was interest in analyzing data for a less typical sorbent. Sodium polyacrylate is categorized as a superabsorbent polymer due to its ability to retain potentially hundreds of times its dry weight in fluid (water) [6] that could be used for absorption cooling. In contrast to zeolite, sodium polyacrylate can absorb refrigerants as either a gas or a liquid, making it even more versatile than more traditional adsorbents. In order to determine the feasibility of this material for cooling applications, the fundamentals of this material must be understood.

Sodium polyacrylate is a polymer with the chemical formula $[-CH_2-CH(CO_2Na)-]_n$ [7] and has been commercially available for many years for applications such as diapers, thickening agent, and waste water clean-up. This material is particularly well-suited at absorbing pure water and does so via hydrogen bonding. Given the polar nature of water molecules and the exterior hydrogen atoms, water molecules very readily are absorbed. A visual depiction of this process is shown in Figure 1.3 [8]. It can be noted that each branch of the polymer chain can bond to a water molecule which is why so much water can be absorbed relative to the amount of dry mass of polymer is provided. This polymer can be made in bulk relatively cheaply, which also make it an appealing alternative to some other more traditional sorbents.

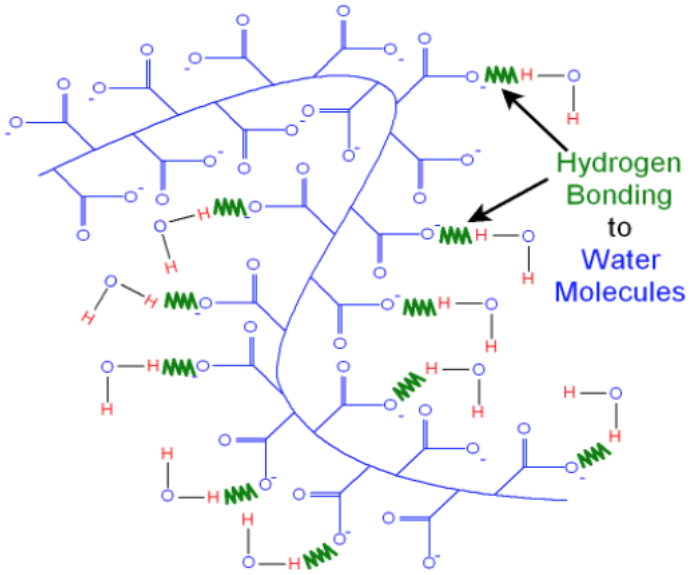

Figure 1.3: Hydrogen Bonding between Pure Water and Sodium Polyacrylate [8]

1.4 Utilizing Ultrasound to Enhance Desorption Process

In adsorption refrigeration, the main weakness of the cycle is the time and amount of energy required to regenerate the sorbent. For this reason, there have been several studies completed using novel methods to assist the desorption process such as using microwave heating [9] [10] and ultrasonic energy [11] [12]. In particular, the ultraonic approach to adsorbent regeneration is the subject of growing interest in the refrigeration community. Since the desorption process is a significant barrier to widespread implementation of adsorption refrigeration, a more fundamental understanding of the desorption process must be developed before novel solutions can be evaluated.

To understand how the implementation of ultrasound in assisting the desorption process, first the significant metrics must be defined. The most obvious of these is

the desorption rate (DR) which is defined as the mass desorbed over time

$$DR = \frac{m(t)_{n+1} - m(t)_n}{(t_{n+1} - t_n) * (m_i - m_{dry})} \tag{1.3}$$

Where m_i is the initial mass of the adsorbent with refrigerant, $m(t)_{n-1} - m(t)_n$ is the time varying mass difference of the adsorbent and refrigerant, and $(t_{n+1} - t_n)$ is the time step over which desorption occurs. The units for this metric is t^{-1} to make it as general as possible. Even with this normalizing by system mass, the desorption rate is not as useful when comparing systems with different masses of adsorbent and refrigerant due to the sensitivities of the measurement, so another useful, normalized metric to compare between these types of system is the percentage of refrigerant desorbed. This metric can be defined as

$$\%\ desorbed = \left(\frac{m_{desorb}(t)}{m_i X_{H_2O}}\right)100 \tag{1.4}$$

Where X_{H_2O} is the mass fraction of the refrigerant in the system and m_{desorb} is the total amount of mass desorbed as a function of time. This value can be compared over time between systems whose masses may not be the same. Two more useful terms that can be used to characterize the system are defined efficiencies for the ultrasonic energy (UE) and the total energy (TE). Expressions defining these terms are shown in equations 1.5 and 1.6.

$$UE = \frac{(m(t)_{n+1} - m(t)_n) l_f}{(t_{n+1} - t_n)\dot{P}_{US}} \tag{1.5}$$

$$TE = \frac{(m(t)_{n+1} - m(t)_n) l_f}{(t_{n+1} - t_n)(\dot{P}_{US} + \dot{Q}_{in})} \tag{1.6}$$

where l_f is the specific latent heat of evaporation. These two terms describe how effectively energy input (in terms of ultrasound and total energy provided) is at driving desorption.

Work that has been previously done in ultrasound-assisted desorption in sorbents

[11] [12] has been done using silica gel as the sorbent and performing experiments framed around using ultrasound to lower the regeneration temperature of that material. The results that were obtained were positive showing that introducing ultrasound into the desorption cycle did indeed cause a reduction in the regeneration temperature as shown in Figure 1.4 [12]. These results clearly show the amount of desorption that occurs in the presence of ultrasound is significantly greater than desorption that occurs without ultrasound, for the same warm air flow temperature. A proposed mechanism for this result of improved regeneration at lower temperatures due to the ultrasound exciting the gas molecules within in sorbent such that they require less thermal energy to be released. However, the amount of energy transmitted to the sorbent via heat transfer was not measured, so no definitive conclusions could be made on whether utilizing ultrasound would be more efficient from an energy perspective than just using the corresponding energy in the form of heat. The goal of this study is to make an experiment capable of showing whether or not it would make sense to use ultrasound to assist the desorption process from an energy perspective, rather than strictly temperature.

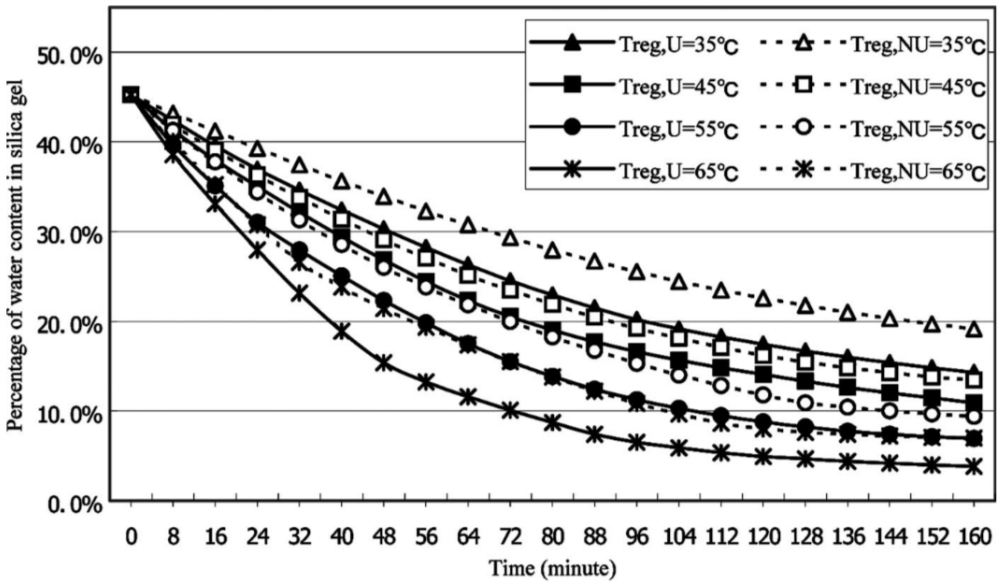

Figure 1.4: Results from Previous Study of Ultrasound Assisted Desorption in Silica Gel [12]

1.5 Adsorption Cooling

Though the focus of this study is around improving just the desorption process, the desired application is for use in adsorption cooling. With that in mind, a brief overview of adsorption cooling will be provided here. A schematic and Clapeyron diagram of a simple adsorption cycle is shown in Figures 1.5 and 1.6 [13]. This cycle consists of four processes. First, the saturated adsorbent is heated causing the pressure to increase from the evaporating pressure to the condensing pressure. Next, a valve between the adsorbent bed and the condenser opens while continuing to apply heat, but now at constant pressure. After that, the valve connecting the adsorbent bed and the condenser is closed and the vapor rejects heat to a cooling fluid which will also reduce the pressure back to the condensing pressure. The valve connecting the condenser and the evaporator is then opened allowing the condensed fluid (at low pressure) to enter the evaporator. Finally, the valve connecting the condenser and

the evaporator is closed and in the evaporator the refrigerant extracts heat from the ambient (this is the refrigeration load) which boils the refrigerant which is then routed to the adsorbent bed to resaturate the adsorbent. By this process, refrigeration can be generated using only heat as opposed to the vapor compression cycle which requires pump work. The purpose of this study is to investigate if the time and heat required to regenerate the sorbent material could be improved by utilizing ultrasonic energy. The potential impact these two parameters can have on an adsorption cooling cycle is clear based on the traditional defintion of the coefficient of performance of a heat pump [14]

$$COP_{HP} = \frac{Q_{out}}{Q_{out} - Q_{in}} \tag{1.7}$$

where Q_{out} is the heat energy rejected from the system and Q_{in} is the heat energy supplied. For an adsorption refrigeration cycle with constant heat input, the Q_{in} is defined as

$$Q_{in} = \dot{Q}_{in}\Delta t \tag{1.8}$$

It is clear from equations 1.7 and 1.8 that if Q_{in} is reduced (which can be accomplished by decreasing the Δt required to achieve Q_{in}) that if COP of the cooling cycle will increase.

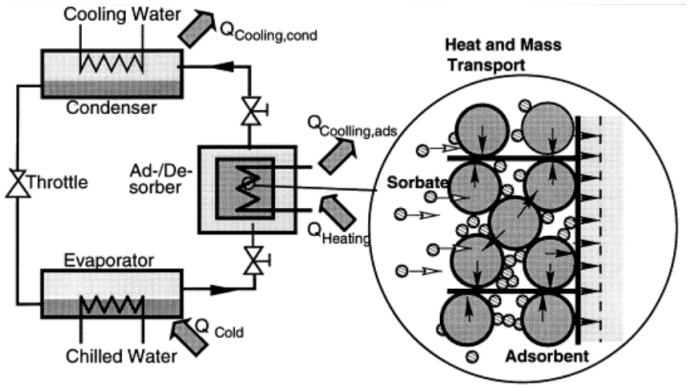

Figure 1.5: Schematic of Simple Adsorption Refrigeration Cycle [13]

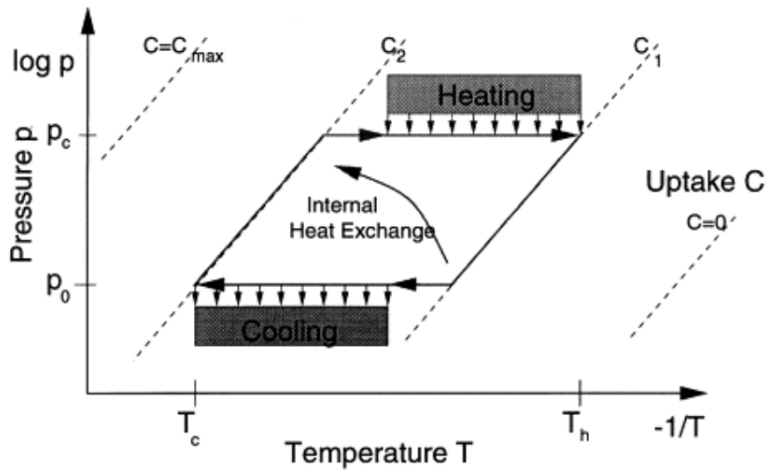

Figure 1.6: Clapeyron Diagram for Simple Adsorption Refrigeration Cycle [13]

Chapter 2

APPROACH

2.1 Design of Ultrasound Enhanced Desorption Experiment

In order to determine whether or not the use of ultrasound has any effect on a desorption process, an apparatus designed to supply ultrasonic acoustic energy and heat to a sorbent must be constructed. Given the diverse physical phenomena that this vessel will be simultaneously subject to during this experiment, special considerations must be made to the material selection and the experiment configuration. The goal of the experimental design is to arrange a system where heat and ultrasound can be applied to a sorbent while temperature at various locations is being measured and stable weight readings can be easily obtained over time.

2.1.1 Material Selection

There are several factors that must be considered when selecting a material for use in an ultrasonic application. In the experiment under discussion, both heat and ultrasonic energy are applied to a bed filled to some degree with a sorbent material. The challenge in this is finding a bed material that will insulate the bed to minimize the potential for heat loss but also reduces the ultrasound's attenuation to the environment. In this case, high density polyethylene (HPDE) was chosen to construct the adsorption bed due to its relatively low thermal conductivity, acoustically insulative properties due to low stiffness, and ease of fabrication. Additionally, HDPE has another advantage in that it can transmit certain wavelengths of infared (IR) radiation which enables non-contact temperature measurement to more thoroughly character-

ize the temperature profile. The percentage of infared radiation transmission as a function of wavelength is shown in Figure 2.1 [15].

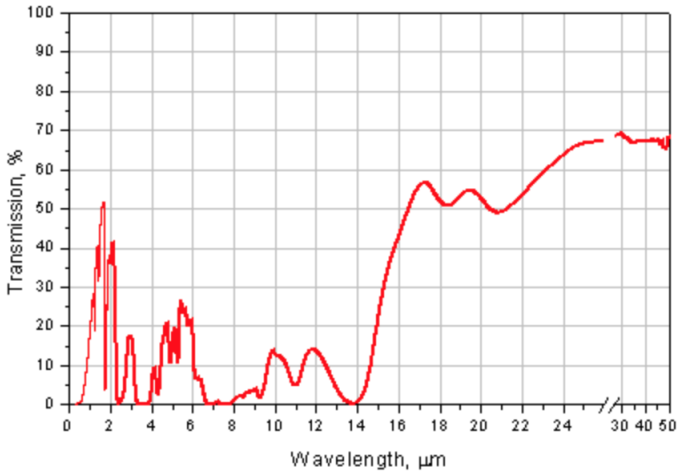

Figure 2.1: Infared Transmission Through a 2mm Thick Sample of HPDE as a Function of Wavelength [15]

Though the IR transmission properties of HDPE are not quantitatively taken advantage of for this experiment, utilizing this material has the potential to allow a more fundamental understanding of the transport phenomena at work in this system to be developed in the future as this research area becomes more mature. It is worth noting that in order to take advantage of the IR transmission properties of HPDE that the heat source would have to be generating heat either at about 1.5 microns or greater than 16 microns based on Figure 2.1.

Coupled to the adsorption bed is an acoustic energy source. Though there are many methods that can be used to supply acoustic energy into a system, for this experiment using a piezoelectric element to generate ultrasonic sound waves was selected due to this technology's robust performance and relative low cost. There is a wide assortment of commercially piezo transducers available, but in the application of desorption (transmitting ultrasound to a sorbent) there are certain material prop-

erties of the piezo that must be given special consideration. The aim of the adsorbent bed/piezo design will focus on maximizing the amount of ultrasonic energy imparted to the sorbent rather than the bed. Key piezoelectric parameters that must be contemplated include the Curie temperature, the electromechanical coupling factor, and available transducer geometries.

The Curie temperature (T_C) is a temperature that if a ferromagnet (such as a piezoelectric transducer) is heated above it, the thermal energy is sufficient to overcome the molecular forces that impose the permanent magnetic properties [16]. Furthermore, it is a recommendation by ultrasonic transducer manufacturers that the temperature of the piezoelectric during operation not exceed roughly half of the Curie temperature [17] to maintain consistent performance. For this experiment where heat and ultrasound are being simultaneously applied, the piezo was selected to ensure that the half of the Curie temperature was within the range of the regeneration temperature of the sorbent material. Otherwise, experimental results may not be repeatable or consistent between trials.

Another important property of the piezo that must be considered is the electromechanical coupling factor (k_t). This unitless material constant is a measure of a piezoelectric's ability to convert electrical energy into acoustic energy with a value of one representing perfect conversion. This factor is different from what the efficiency of the piezoelectric is since this factor does not account for dielectric or mechanical losses [17]. This factor is defined mathematically as [18]

$$k_t^2 = \frac{e_{33}^2}{c_{33}^D \epsilon_{33}^S} \tag{2.1}$$

Where e is the piezoelectric charge constant, c^D is the elastic compliance under electric displacment, ϵ^S is permittivity under strain. This factor is not the same in all directions (as denoted by subscripts in equation 2.1) which must be considered. A

typical coordinate system is shown below in Figure 2.2 and for the purposes of this experiment the primary direction of concern will will be vibrations in direction 3 which informs the piezoelectric selection process.

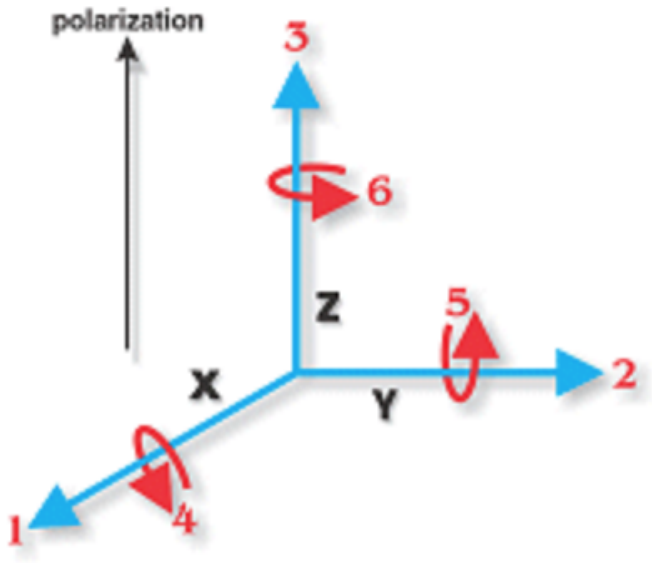

Figure 2.2: Typical Coordinate System for Piezoelectric Element [17]

Finally, when selecting a piezoelectric for use in a desorption bed there are practical geometric constraints that must be considered. Custom piezoelectric transducer geometries are available for order to accommodate any desired specifications, but this option is cost prohibitive, and generally will have less empirical data available from the manufacturer given the custom nature of the part. For this reason, an "off the shelf" piezoelectric was chosen. In order to maintain constant ultrasound distribution through the sorbent (not the bed or heater) a ring type transducer was chosen. This type of transducer is designed to generate ultrasound in the 3 direction shown in Figure 2.2 from the top surface of a ring which has a thickness, inner, and outer diameter. A diagram more clearly showing this arrangement will be presented in the next section. A summary of the dimensions and properties of the piezoelectric

element is shown below in table 2.1 along photograph of the actual transducer that was used in the experiment shown in Figure 2.3.

Table 2.1: Piezoelectric Element Dimensions/Properties

Parameter	**Value**
Type	Ring
Material	APC 842
Outer Diameter	50 mm
Inner Diameter	20 mm
Thickness	6.35 mm
Curie Point (T_C)	325°C
Electromechanical Coupling Factor (k_t)	0.48

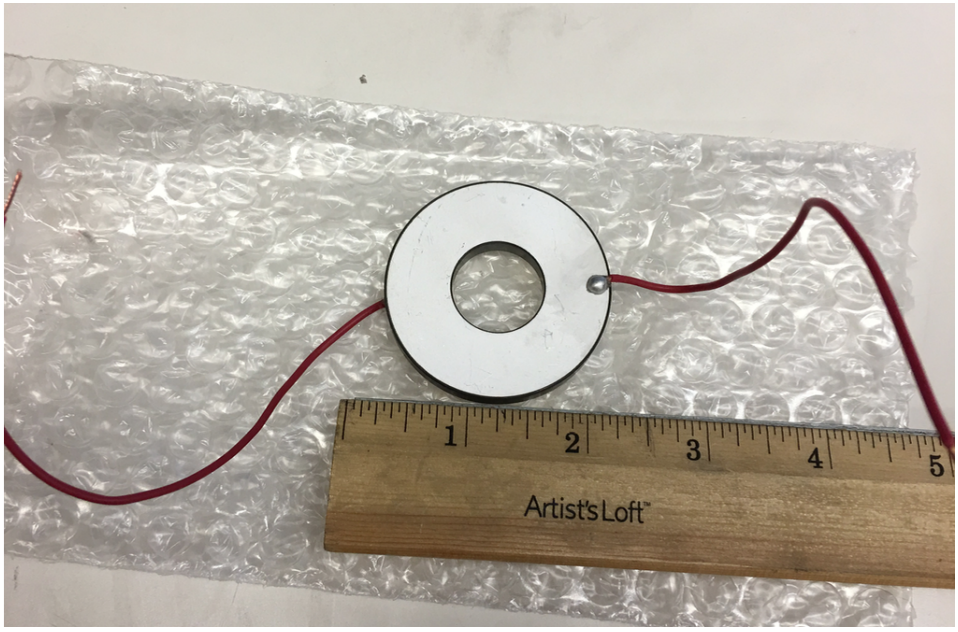

Figure 2.3: Photograph of Piezoelectric Element used in Desorption Trials

2.1.2 Experiment Configuration

Once all material selection is completed, the overall configuration of the experiment can begin to take shape. As previously stated, the main goal of this design is to create an environment in which heat and ultrasound can be simultaneously applied to a sorbent while collecting temperature and mass change data. Ideally, the system components supplying heat and ultrasound will interact as little as possible to ensure repeatable results. All design decisions were made based on these constraints which is clear in the final experiment and the results.

Before design of the desorption bed began, the heat source and piezoelectric element was selected since they dictate the geometry the bed itself must be made. For the heat source, a cartridge heater was selected due to its ease of use only requiring a DC power supply to operate and its reliability in generating a specified heat flux. An alternative that was considered was using resistance heating wire, but based on previous experience this is suboptimal since heater wire is less able to maintain a constant heat flux as it heats up and it is difficult to get a uniform flux area into the sorbent based on the small cross-sectional area that the wire has. Coupled with the cartridge heater is a ring-type piezoelectric element. A ring-type element was selected to ensure that the acoustic energy generated was transmitted to the sorbent as much as possible, rather than into the heater. A qualitative path of the heat and acoustic power is illustrated in Figure 2.4.

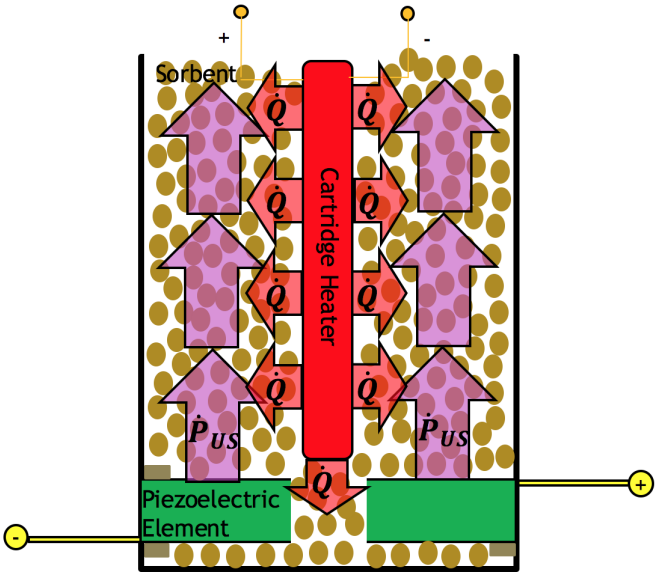

Figure 2.4: Cartridge Heater and Ring-Type Piezoelectric Element Configuration Schematic

From this conceptual design, a final dimension for the desorption bed was determined. Since the piezoelectric element selected was round, the bed correspondingly was made cylindrical to allow the element to be easily placed in the bed. A cylindrical bed was machined out of cylindrical HDPE with an inner diameter to allow a slip fit of the selected piezoelectric, an outer diameter to allow the wall thickness to be sufficiently thin to have adequate IR transmission, and an overall length to allow the cartridge heater to fully fit inside the bed to allow all heat generated by it to be transferred to the sorbent. This design essentially allows all heat from the cartridge heater and all acoustic energy generated by the piezoelectric to be transferred to the adsorbent. Any heat generated by the piezoelectric element itself or by the sorbent while attenuating the ultrasound is considered negligible.

In order to maximize the amount of acoustic energy transferred from the piezoelectric to the sorbent, it became clear that putting the element in a "floating" con-

figuration would be best. A floating configuration means that the piezoelectric does not have fixed constraints on any point on it which allows it to freely vibrate while being encompassed by a surrounding medium. This was accomplished by integrating an air gap at the bottom of the bed to allow minimal interaction between the piezo and the structure of the bed. Physically this was done by drilling through two secant lines near the bottom of the bed (on the diameter) and placing wooden rods through the bottom of the bed on which the piezoelectric sits. Wood was selected as the material due to its low thermal conductivity, low mechanical strength relative to the piezoelectric, and ease of implementation. A third wooden rod was also used to potentially retain the piezoelectric from the top in case the acoustic energy was large enough to cause the piezo to jump out of the bed, but since this pin was not in physical contact with the top surface, the float principle still holds.

In addition to fixing the position of the piezoelectric, fixing the position of the cartridge heater was also an important design feature of the desorption bed. If the heater could remain in the bed during the entirety of the experiment, an important aspect to consider is how the heater may move in a bed subject to sonication. To mitigate this risk of uncertainty of the heater's position with respect to the bed, three glass pins oriented 120° from each other were used to triangularly retain the heater in the center of the bed. In this case, glass was selected instead of wood due to it's relatively low thermal conductivity and ability to sustain the high temperatures that would result when in contact with the heater. The height of the bed was determined based on the heaters available and the weight constraints of the scale that was used to measure the mass. A basic drawing with these design features and basic dimensions below are shown in Figure 2.5.

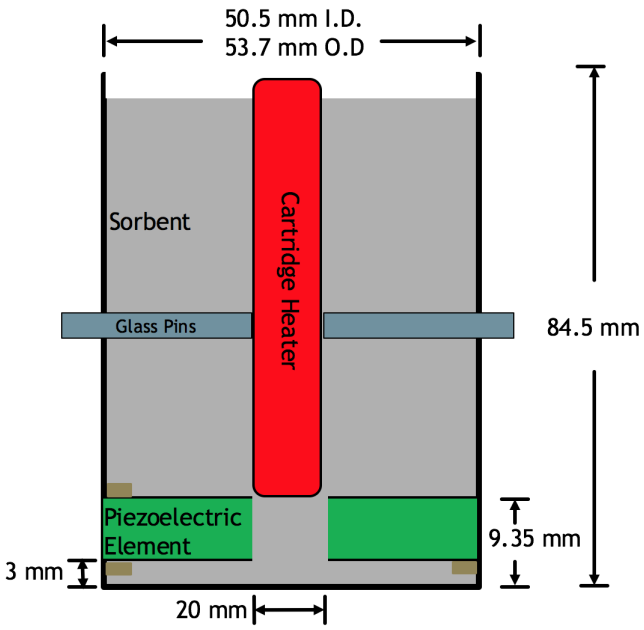

Figure 2.5: Drawing of Desorption Bed, Heater, and Piezoelectric Element with Basic Dimensions

Ensuring that the bed is well insulated and reliable temperature measurements could be at multiple locations within the bed were also of concern while constructing the bed. Seven small holes were drilled into the bed to allow thermocouples through to develop a thermal profile while the experiment was being conducted (this will be discussed in greater detail later in this chapter). Additionally, insulated PVC foam pipe wrap was cut to size and stuck all along the outer surface of the bed to minimize heat transfer from the bed to the environment. Finally, for the zeolite experiment a thin sleeve to be placed on the inner diameter of the bed was machined out of Renshape®460 (a glass reinforced mold material) to both further insulate the bed and also to protect the HDPE from melting which was a concern in higher heating power experiments. Renshape was used due to its high working temperatures, ease of fabrication, and material availability.

2.2 Data Acquisition

Obtaining stable and reliable data is the cornerstone of any experiment and this study is no exception. Of primary interest to measure in this experiment was the change in sorbent mass over time, the temperature at various points in the bed, the input heating power, and the input power to the piezoelectric. In a cooling application, the pressure is also necessary to measure, but since this experiment is only concerned with the desorption process which is open to atmosphere, obtaining pressure data was not of significant concern. The methods used to record the experimental data are robust and there can be confidence in any conclusion drawn from the data, though a brief discussion of the method used to measure each parameter may provide the reader insight into how such an assertion can be made.

The mass change over time of the sorbent in the desorption bed was measured using the very traditional means of using a digital scale and a stopwatch. Though rudimentary in nature, this method proved to be the most robust and convenient for obtaining real-time experimental data. Due to the various wires that were attached to the desorption bed (thermocouples, cartridge heater power supply, and ultrasonic power supply), there was significant fluctuation in the readings of the scale when taking measurements. In situations where these fluctuations were observed (notably significant in zeolite experiments), it was determined that the best way to obtain reliable mass data when these fluctuations we present was to remove the heater and disconnect the ultrasonic power wires when taking the measurement. Ideally, the thermocouple wires would also be removed when measuring mass, but doing so would cause too much uncertainty in the placement of the thermocouples to have confidence in the temperature data. Non-removable thermocouples could have caused uncertainty in the mass measurements if the thermocouples formed a coating over the

course of the experiment, but this was not observed based on microscope inspection. For zeolite trials, the desorption bed was placed on the scale to obtain measurements after the heater was removed and then taken off the scale to re-situate the heater. For sodium polyacrylate trials, the desorption bed was kept on the scale for the duration of the experiment in an effort to improve measurement stability. The digital scale (model) was used to measure the mass at a set frequency during the experiment and those data were manually recorded for use in later analysis.

Temperature data in the desorption bed was collected from seven locations using thermocouples and an Omega DAQ-2400. Five of the thermocouples were placed at the midpoint between the bed wall and the heater inline with each other in order to evaluate the longitudinal temperature profile during the desorption process. Of the two remaining thermocouples used, one was placed near the bed wall and the other was placed near the heater. These two thermocouples in conjunction with one of the five longitudinal measurements can be used to evaluate the radial temperature profile. A diagram indicating thermocouple placement within the bed is shown in Figure 2.6.

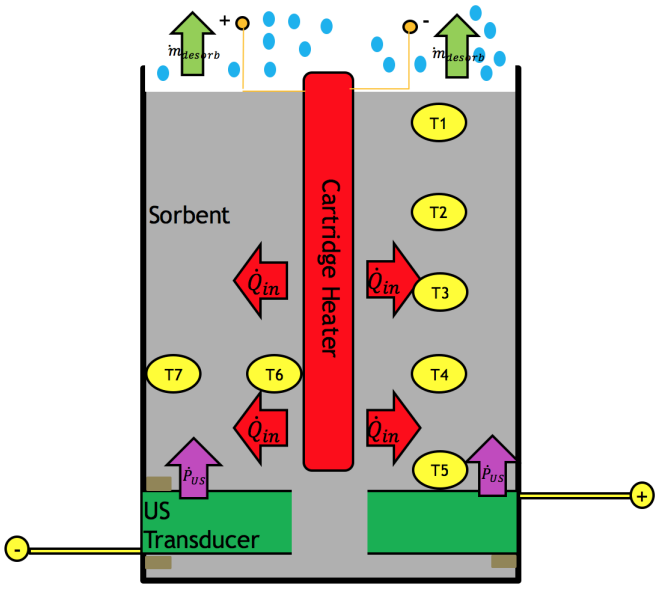

Figure 2.6: Diagram of Thermocouple Placement Within Desorption Bed

Additionally, ambient wet bulb temperature data was collected for each trial in conjunction with the ambient temperature (read from a thermometer) to calculate the relative humidity conditions of the atmosphere at the time of the trial to ensure consistency between runs.

From the design phase, the material selection was made, in part, around the fact that HDPE is transmits certain wavelengths of the IR spectrum that may be used for temperature measurements. However, as the experimental setup was being validated, it was observed that the IR camera available was not giving reasonable temperature readings through the HDPE bed wall likely due to the set wavelength range of the camera. Additionally, the exact emissivity of the outer bed wall is unknown and would be difficult to measure empirically. For this reason, IR camera readings were not used as a primary temperature measurement technique, but this will likely be adapted to support future work.

Measuring the input heating power provided by the cartridge heater was trivial due to the simple heating model that was assumed. Since the heater is fully enclosed by the sorbent and the conversion efficiency between electricity to heat can be assumed near 100% efficient, it stands to reason that all of the input electrical power ($\dot{P}_{elec}$) can be considered to be converted to input heating power ($\dot{Q}_{in}$). This value was actually measured as the output power of the DC power supply using the equation defining electrical power in a DC circuit shown in equation 2.2.

$$\dot{P}_{elec} = V_{measured} * I_{measured} \cong \dot{Q}_{in} \tag{2.2}$$

Where $V_{measured}$ is the measured DC voltage from the power supply and $I_{measured}$ is the measured current output from the power supply. These quantities were measured by the power supply itself and validated with a Fluke digital multimeter.

Empirically obtaining the ultrasonic power produced by the piezoelectric element

is possible [19], but can be difficult to do without the proper equipment and expertise. For this reason, instead of attempting to measure the ultrasonic power directly, the input power to the piezoelectric was measured and considered in the results. This is in agreement with the energy approach that is being taken in this study though it is noted that measuring the ultrasonic power directly would be ideal. Measuring the input power to the piezoelectric is not a trivial task, but it can be done with care if an appropriate configuration is used. To understand an adequate set-up to measure the AC power, recall the analog to Ohm's law for alternating current.

$$V_m sin(\omega t) = Z I_m sin(\omega t - \phi) \tag{2.3}$$

Where V_m is the average voltage, I_m is the average current, Z is the impedance, ω is frequency, t is time, and ϕ is the phase angle between the voltage and current. Equation 2.3 is very similar to the definition of Ohm's law for a DC circuit except for the phase angle component, ϕ. If $\phi = 0$, then the standard Ohm's law relation would apply since the impedance Z is equivalent to the nominal resistance R when the voltage and current are in phase, as is the case with direct current:

$$V_m = R I_m \tag{2.4}$$

The circuit is in-phase when the frequency of the alternating current is equal to the resonant frequency of the constituent components ($\omega = \omega_r$). When the circuit is operating at the resonant frequency, then equation 2.2 can be used to calculate the power consumed by each component, such as the piezoelectric element. Now that the mathematical relationship between alternating current, voltage, and resistance is known in the context of the resonant frequency, there are several questions that must be answered before the power input to the piezoelectric can be calculated: what is the voltage drop across, the current drawn by, and the resonant frequency of the

piezoelectric element?

The voltage drop across the piezoelectric is a simple enough thing to compute. Using an available oscilloscope and two voltage probes, the input and output voltage can be measured and the voltage drop across the piezo is simply the difference between these two values. To find the current drawn is a more complex problem. In order to do this, a shunt resistor must be implemented in the circuit. A shunt resistor is a resistor of small, known magnitude that if put in series with the piezo, the known resistance and measured voltage drop can be used in Ohm's law (equation 2.4) to calculate the current. By Kirchoff's Current Law, the current that goes through the piezo and the shunt resistor must be the same. Thus, by using an oscilloscope and a shunt resistor, both the voltage drop across and the current drawn by the piezo can be calculated. However, equation 2.2 only applies in an AC circuit at the resonant frequency, which is needs to be determined. The procedure to measure the resonant frequency is detailed in the next section.

2.2.1 Measuring the Resonant Frequency of a Piezoelectric Element

The resonant frequency of a piezoelectric element depends upon the material it is made of, its geometry, and any coupling affects from whatever it is vibrating with. Occasionally, manufacturers will give a value of the resonant frequency of a particular piezoelectric element in their catalog, but this is the resonant frequency if the element is free to vibrate in air. For most applications, this value will not suffice since even if the resonant frequency is altered slightly by the application, it can greatly effect how efficiently electrical energy is converted into mechanical waves. Since the resonant frequency is the frequency at which the piezo is most efficient [17], it is very valuable to measure the resonant frequency in the application it is intended. For the purposes of this study, measuring the resonant frequency of the piezoelectric element inside the

desorption bed surrounded by sorbent is imperative.

To measure the resonant frequency is to measure at what frequency the output voltage from the piezoelectric is in-phase with the input signal. To do this, a circuit was built as shown in Figure 2.7.

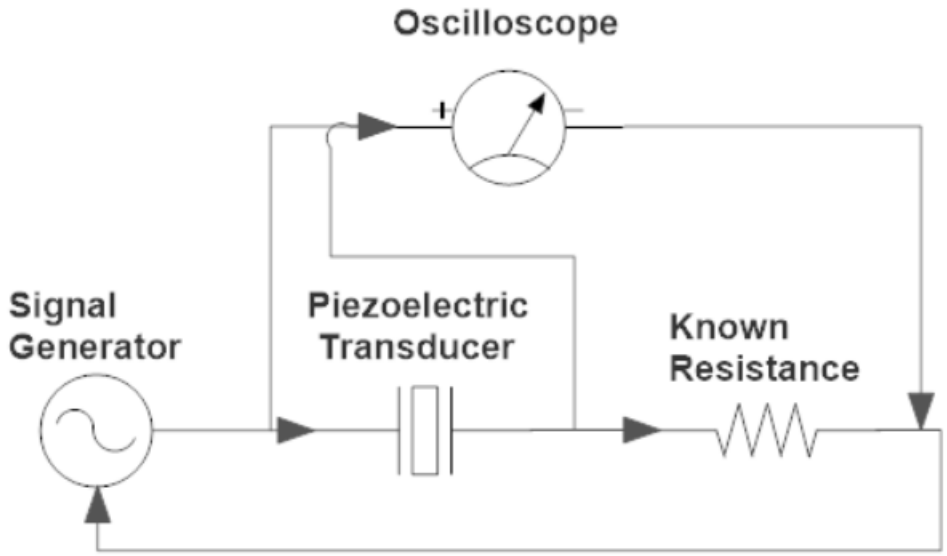

Figure 2.7: Circuit Used to Measure the Resonant Frequency of the Piezoelectric Element in the Desorption Bed

Once the circuit in Figure 2.7 was constructed, a constant voltage amplitude was set from the signal generator (V_{SG}) and the oscilloscope displayed the waveforms of the output signal of the signal generator and the output voltage drop across the shunt resistor (V_R). As the frequency on the signal generator is varied, the amplitude of the output from the signal remains the same, but it is noted that the voltage drop across the piezoelectric and shunt changes with the frequency. This is visibly noticeable in the waveform, as well. Starting in the ultrasound domain (over 20kHz), it can be observed that the voltage drop across the shunt will reach a maximum value at a certain frequency and then begin to decline. The frequency corresponding to the

maximum voltage is the resonant frequency. Figure 2.8 shows the waveforms of the output voltage from the piezo, just before resonance, at resonance, and just after resonance.

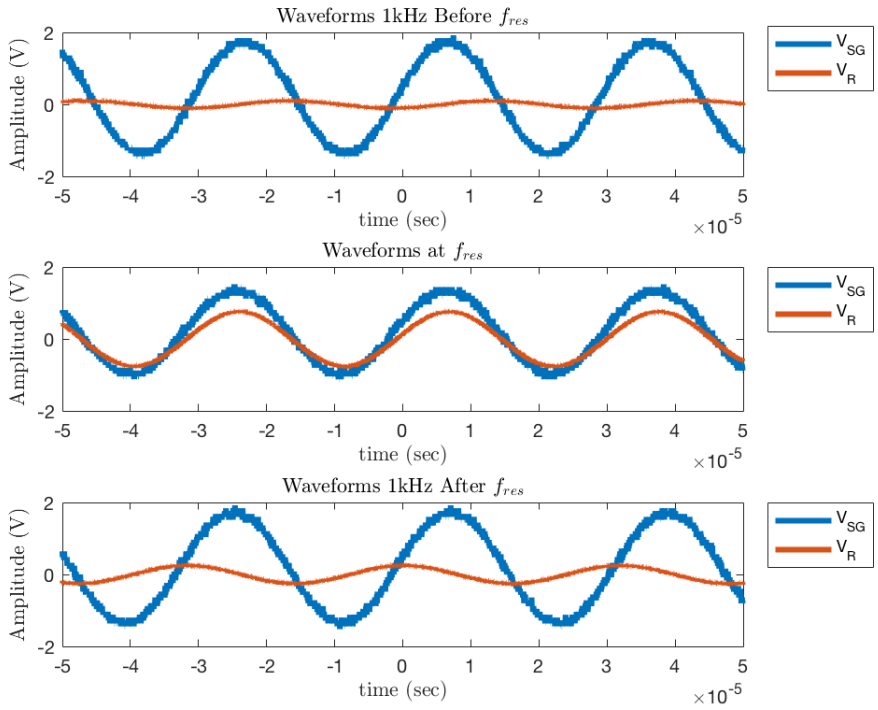

Figure 2.8: Waveforms of Signal Generator Voltage (V_{SG}) and Voltage Across Known Resistance (V_R) before, at, and after Resonance

It is clear from the waveforms that at the resonant frequency, V_{SG} and V_R are in-phase (maximum values for amplitude occur at the same time step) with each other which makes sense based on earlier discussion. It is also clear from the waveforms that there is a sharp decrease in the piezoelectric voltage even if the signal is relatively near the resonant frequency (within 1kHz). To visualize this drop off, many frequencies were tested and their corresponding voltage was plotted for the case of an empty bed and the case of a bed full of sorbent. The result is shown in Figure 2.9 indicating that in

this particular case the resonant frequency occurs at 32.9 kHz.

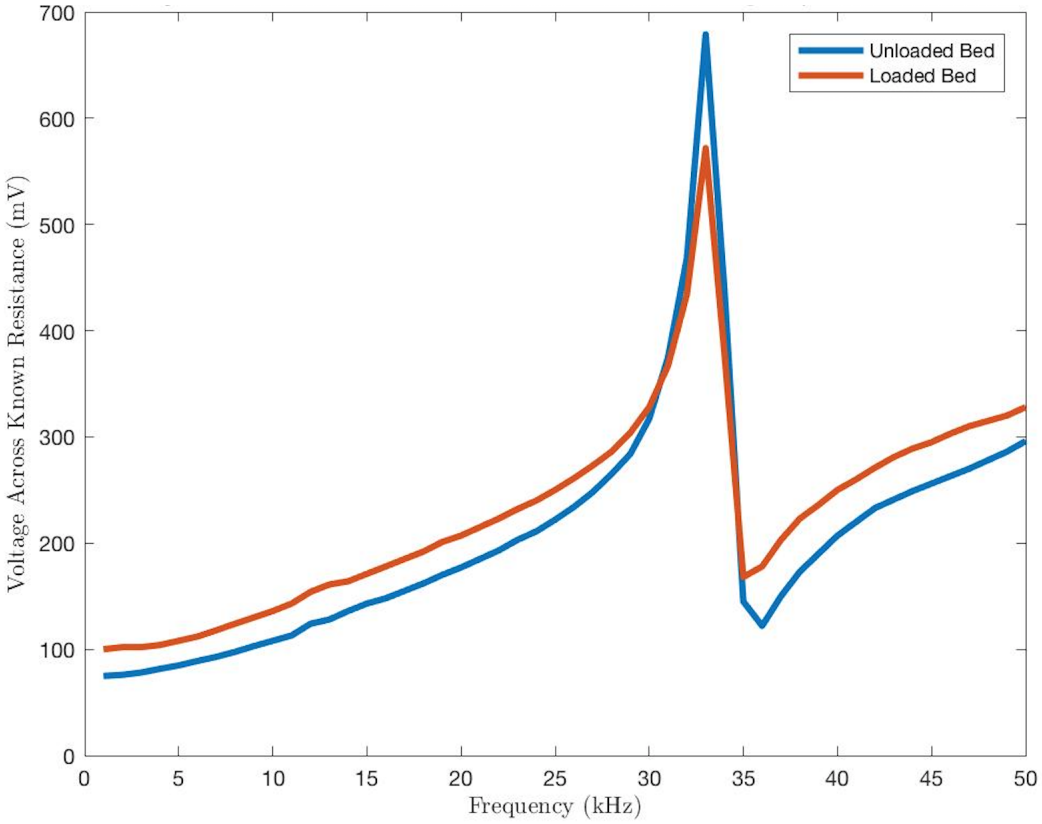

Figure 2.9: Piezoelectric Output Voltage as a Function of Frequency

Now that a method for establishing the resonant frequency has been established, all parameters required to measure the input power to the piezoelectric element are known. With this information, robust methods for comparing desorption on an energy basis between heat and ultrasound can be completed while keeping inherent uncertainties as part of the solution.

2.3 Uncertainty Analysis

Calculating the uncertainty of measurements is a very important part of any experimental study. Only after uncertainty in measurements has been shown to be sufficently low can any conclusions be presented with confidence. In general, the

uncertainty of experimental data can be broken into two parts, the bias error and the precision error [20]. There are well understood methods for determining both error components that will be used in the next two sections to determine how uncertainty will figure into the final results.

2.3.1 Bias Error

To determine the bias error of experimental data, Taylor's Theorem can be applied. If a parameter (y) is calculated using parameters that are primary measurements (x_n) such that

$$y = f(x_1, x_2, ..., x_n)$$

the uncertainty of the calculated parameter (Δy) can be defined as shown in equation 2.5 [20]

$$\Delta y = \sqrt{\left(\frac{\partial f}{\partial x_1}\right)^2 * (\Delta x_1)^2 + \left(\frac{\partial f}{\partial x_2}\right)^2 * (\Delta x_2)^2 + ... + \left(\frac{\partial f}{\partial x_n}\right)^2 * (\Delta x_n)^2} \tag{2.5}$$

To determine the uncertainties of relevant calculated parameters such as desorption rate, ultrasonic efficiency, total efficiency, and percent water desorbed, equation 2.5 can be used as a model. Take for example, equation 1.3. Relevant derivatives can be calculated from that equation, the results being shown in equations 2.6 to 2.11.

$$\frac{\partial DR}{\partial m_{n+1}} = \frac{1}{(m_i - m_{dry})(t_{n+1} - t_n)} = a \tag{2.6}$$

$$\frac{\partial DR}{\partial m_n} = \frac{-1}{(m_i - m_{dry})(t_{n+1} - t_n)} = b \tag{2.7}$$

$$\frac{\partial DR}{\partial m_i} = \frac{-(m_{n+1} - m_n}{(m_i - m_{dry})^2(t_{n+1} - t_n)} = c(t) \tag{2.8}$$

$$\frac{\partial DR}{\partial m_{dry}} = \frac{(m_{n+1} - m_n}{(m_i - m_{dry})^2(t_{n+1} - t_n)} = d(t) \tag{2.9}$$

$$\frac{\partial DR}{\partial t_{n+1}} = \frac{-(m_{n+1} - m_n}{(m_i - m_{dry})(t_{n+1} - t_n)^2} = e(t) \tag{2.10}$$

$$\frac{\partial DR}{\partial t_n} = \frac{(m_{n+1} - m_n}{(m_i - m_{dry})(t_{n+1} - t_n)^2} = f(t) \tag{2.11}$$

To help keep future forms of the uncertainty equation compact, the derivatives above were abbreviated using english letters and the notation if that derivative is a function of time. Equations 2.6 through 2.11 can now be substituted into equation 2.5 to calculate the uncertainty of the desorption rate as shown in equation 2.12.

$$\Delta DR_{bias} = \sqrt{a^2\Delta m_{n+1}^2 + b^2\Delta m_n^2 + c(t)^2\Delta m_i^2 + d(t)^2\Delta m_{dry}^2 + e(t)^2\Delta t_n^2 + f(t)^2\Delta t_{n+1}^2} \tag{2.12}$$

Each term preceded by a Δ is the given bias uncertainty of that measurement. This number is generally given by measurement equipment manufacture and a table showing the documented bias uncertainty for each parameter is provided in table 2.2.

Table 2.2: Bias Uncertainties Given by Measurement Equipment Manufacturers

Parameter	**Bias Uncertainty**
Δm	$\pm$0.01 g
Δt	$\pm$0.003 min
ΔV	$\pm$2%
ΔR	$\pm$2%

There are no subscripts denoted in table 2.2 since these are the general values for the given equipment and therefore the values can be applied to each specific parameter.

2.3.2 Precision Error

Precision (also called random) error is treated differently than bias error since this error component can stem from experimental elements such as varying environmental conditions and inconsistencies. This kind of error is not given by the manufacturer,

but must be measured by taking measurements that should be consistent and seeing by how much they vary from measurement to measurement. In particular for this experiment, there is a precision error component in that there are wires that lead off of the scale as the bed's mass is being measured. It was observed that since the wires lead outside what should be a closed, coupled system of bed and scale, that these wires will contribute a significant precision error. Quantifying that error can be done by taking several measurements of the desorption bed system while not experiencing desorption and calculating by how much the mass varies within that dataset. A ten measurement sample set is shown in table 2.3 by which a sample precision uncertainty can be calculated.

Table 2.3: Precision Uncertainty Sample Dataset

Measurement	**Scale Reading**
1	263.17 g
2	263.00 g
3	263.00 g
4	263.12 g
5	263.05 g
6	263.02 g
7	263.09 g
8	263.10 g
9	263.07 g
10	263.10 g

From the data in the above table, the mean measured values is calculated to be

$\bar{x} = 263.07$ grams and the standard deviation of the data is $\sigma = 0.055$ grams. If precision error is assumed normal, than iit follows that 95% of observations should fall within $\pm 2\sigma$ of $\bar{x}$ [20]. Thus, the value of 2σ can be used as the precision error of the scale in the experimental data analysis.

2.3.3 Total Uncertainty

It can be shown that the total uncertainty of a measurement is the magnitude of the bias and precision uncertainty components. This can be shown mathematically as shown in equation 2.13.

$$\Delta y_{total} = \sqrt{\Delta y_{bias}^2 + \Delta y_{precision}^2} \tag{2.13}$$

2.4 Experimental Procedure

Now that all factors with design decisions have been discussed and many of practical aspects of the experiment considered, an overview of how the experiments were conducted can be introduced. This will provide the reader with insight as to how data was collected and how consistent the experimental set-up would be between trials.

2.4.1 Sorbent Preparation

Before the experiment can begin, there must be confidence that the properties of the sorbent with some fraction of refrigerant (in this case, pure water) are known. For the zeolite 4A that was used, first the beads were baked at 300°C which is beyond the minimum regeneration temperature for that material [21]. After allowing to bake for one hour, the sample was immediately weighed in order to get a dry mass. Once the dry mass was recorded, the sample was allowed to cool and was then placed in a mesh basket with boiling water underneath. This vaporized water was adsorbed by the zeolite allowing its mass to increase to the saturation point. A diagram illustrating

this process is shown in Figure 2.10.

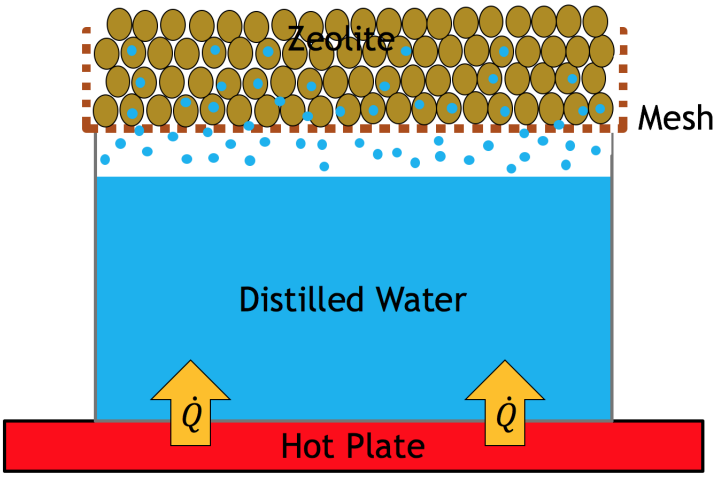

Figure 2.10: Diagram of Zeolite Saturation Process

The saturated sample was then weighed and the water mass fraction (X_{H_2O}) was calculated. For good measure, saturated zeolite samples were kept in a box regulated to 70% humidity. For zeolite, the saturation point does vary with humidity, but stays relatively constant after 50% relative humidity. Figure 2.11 shows how the saturation level of zeolite and several other adsorbents vary with humidity [22].

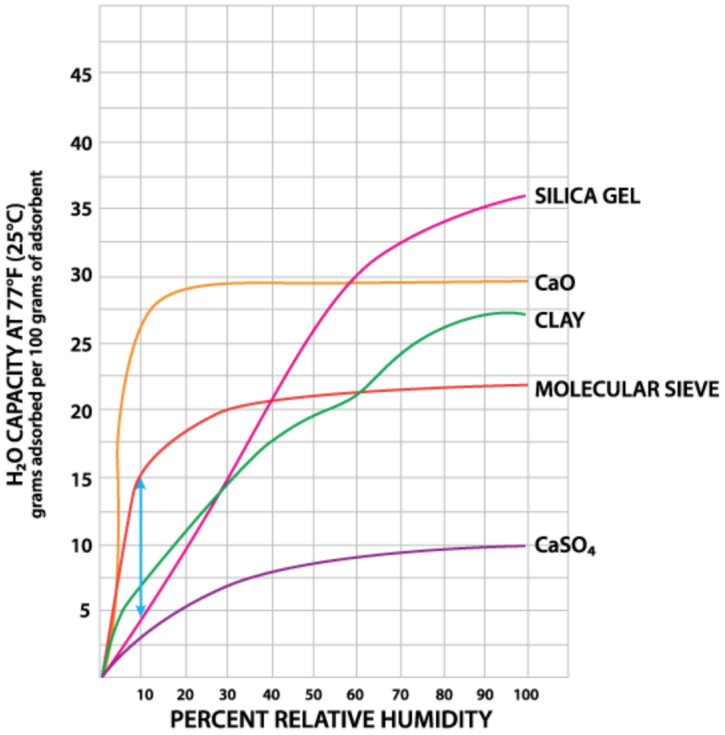

Figure 2.11: Adsorption Capacity of Several Common Adsorbents as a Function of Humidity [22]

The amount of water vapor zeolite could adsorb was repeatably measured as 19.5% of its dry mass which is in good agreement with literature values [21].

For sodium polyacrylate, sample preparation was a much simpler process. The dry mass of the polymer was weighed and a measured amount of pure water was added to the sample. For the experiments conducted, the mass of water added was two hundred times the dry mass of the polymer. Once water was added, the sample was placed into a sealed container and left for 24 hours to ensure all water was absorbed. The polymer was always kept in a sealed jar to ensure there was no natural diffusion of water into the atmosphere (desorption out of the sample) though it was observed that water at room temperature desorbs extremely slowly from this material.

2.4.2 Initial Measurements and Setup

Once the sorbent samples have been prepared, the initial mass of the unfilled bed can be measured and recorded for later use. The thermocouple calibration was then verified using a chilled reference to check thermocouple outputs are accurate. The sorbent was then added (with some known mass fraction of pure water), and the bed's mass would be recorded again as the initial system mass. At this point, the procedure detailed in section 2.2.1 would be used to calculate the resonant frequency of the bed with that specific amount of mass in it. This would be done at low power so as to disturb the system as little as possible before beginning the experiment. This resonant frequency would be used for the duration of that trial. Next, the power to the piezo is turned off and the thermocouples paired with the Omega DAQ are switched on to collect initial temperature data. The thermocouples cannot obtain reliable data while power is being provided to the piezoelectric element since the element generates an electric field that interferes with the thermocouples when power is supplied. Once all of this data was recorded, the experiment could commence.

2.4.3 Performing the Experiment

Upon completing pre-trial data collection, the experiment can begin. First, the piezoelectric element powered by a signal generator in series with an amplifier is set to the resonant frequency. Then, using techniques described in previous sections the power input to the piezo is calculated and set to the desired value. Next, the DC power supply was turned on and the amount of power provided to the heater is set. After both the piezo power and the heater power are set, the stopwatch starts and the trial has begun. Every ten minutes, the heater and piezoelectric element are simultaneously shut off to take mass and temperature measurements. For the

zeolite experiment, the heater is removed and the piezoelectric element wires are disconnected for each mass measurement. This is due to an observed affect of the heater used on the mass measurements as a function of temperature. This effect is likely caused by thermal stress imposed on the wires while at elevated temperatures. This was not necessary in sodium polyacrylate trials, because a smaller heater was used which had negligible effects on the mass reading when at elevated temperatures. This allowed the entirety of the sodium polyacrylate trials to take place atop the scale versus zeolite trials which the scale had to be moved to be underneath the bed every time a measurement was taken. When mass was taken in the case of zeolite, every time the bed was put on the scale, special attention was given to the ensuring the bed was placed in the same orientation on the scale each time. This was accomplished by marking the bed and the scale with indicator marks which were lined up each time a measurement was taken.

It is also worth noting that the input power to the heater and the piezoelectric had to be monitored to ensure consistency. When either of these components input power was turned off, when it was turned back on there frequently needed to be fine adjustments made to verify they were at the correct value. This is especially true of the piezoelectric since the amplifier would alter the frequency ± 0.3kHz by turning it off and back on. In this way, the resonant frequency and resulting power was verified during the entirety of each trial.

2.4.4 Post Experiment

Each trial would last at least ninety minutes. Several longer trials were completed (three hours or more), but it was observed that the desorption enhancement effects of ultrasound are most notable within the first ninety minutes. After the trial duration concluded, the bed was allowed to reach ambient temperature before removing the

sample. This is to protect the wire connections to the piezoelectric which would soften while at elevated temperatures. After reaching room temperature, samples were removed from the bed and stored for potential reuse.

Chapter 3

RESULTS AND DISCUSSION

The results of the several experiments conducted with different sorbents can be interpretted from two perspectives. The first, is to consider the effect the ultrasound had on distributing the heat provided by the cartridge heater. This can be done either by comparing the average temperature at various locations between trials or by comparing the temperature gradient at certain locations between trials. The second perspective to consider is by comparing the mass change data itself, namely in the form of percent of mass desorbed and the desorption rate.

3.1 Zeolite 4A

In order to appropriately analyze the temperature data, a few calculations had to be made prior to generating resulting plots. Since temperature data was only collected at the same frequency as mass measurements (due to the interference of the piezoelectric element on the thermocouple readings) and the heater was removed and reoriented during each measurement, instead of reporting individual thermocouple temperature data an average temperature was used. During the first fifteen to twenty seconds after the cartridge heater and piezoelectric were turned off, the Omega DAQ was turned on and temperature data was collected. After the fifteen to twenty seconds, the heater was removed from the system to take a mass measurement. This heater removal reoriented the sorbent significantly which is evident in the raw temperature data. To better asses the true temperature distribution of the bed while subject to heating and sonication, the raw temperature data from the time period before the heater is removed was averaged to provide a single average temperature data point

at each thermocouple location at the same frequency that mass measurements were collected. This provides a much more robust method for comparing temperature data between trials.

As previously mentioned, temperature data between trials may be best compared when that data is used to show an average temperature or a temperature gradient. For these results, temperature results will be broken up into two general treatments within the desorption bed, the radial and the longitudinal. Refering back to Figure 2.6, it can be noted that there are five thermocouples located in the same radial position at different locations along the length of the bed (T1-T5) and there are three thermocouples located in the same location with respect to the length, but along different locations on in the radial direction (T4, T6, and T7). Only temperature data from the thermocouples in each respective region will be used to calculate the average temperatures and the temperature gradient. It is worth noting that for the longitudinal temperature gradient since the thermocouple T1 is near the ambient, it was not used in that calculation since its reading remained relatviely consistent near room temperature for the entirety of each trial. Instead, T2 and T5 were used to calculate the longitudinal temperature gradient. Thus, the data points shown on the temperature results can be shown mathematically as

$$\bar{T}_{rad} = \frac{T_{T4} + T_{T6} + T_{T7}}{3} \tag{3.1}$$

$$\bar{T}_{long} = \frac{T_{T1} + T_{T2} + T_{T3} + T_{T4} + T_{T5}}{5} \tag{3.2}$$

$$\Delta T_{rad} = T_{T6} - T_{T7} \tag{3.3}$$

$$\Delta T_{long} = T_{T2} - T_{T5} \tag{3.4}$$

It is also noted that there was a communication issue with the Omega DAQ thirty minutes into the 14W heat and 4W ultrasound trial and unfortunately that single

data point was lost on that curve. This did not occur during any other of the trials presented. The results using the experimental data and equations 3.1-3.4 are shown in Figures 3.1-3.4.

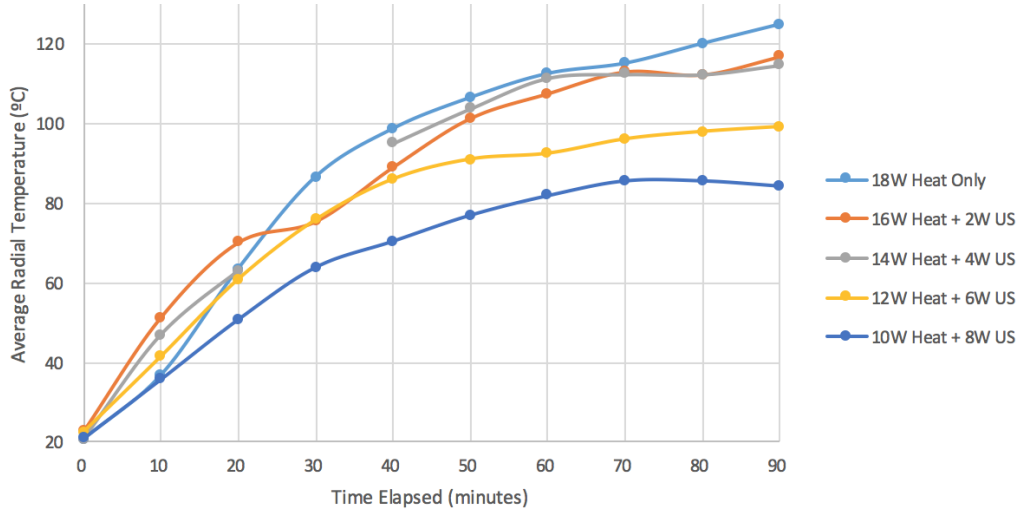

Figure 3.1: Zeolite Average Temperature in the Radial Direction of the Desorption Bed

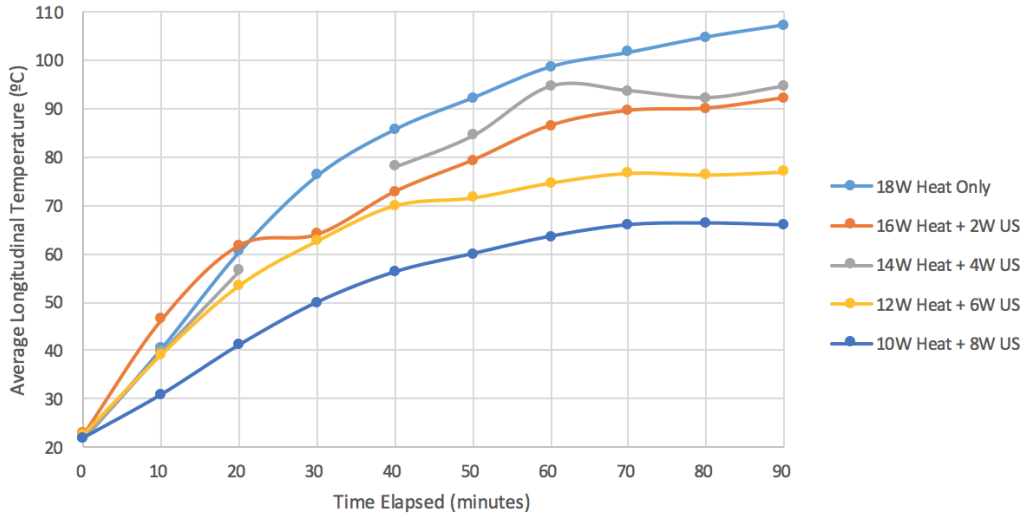

Figure 3.2: Zeolite Average Temperature in the Longitudinal Direction of the Desorption Bed

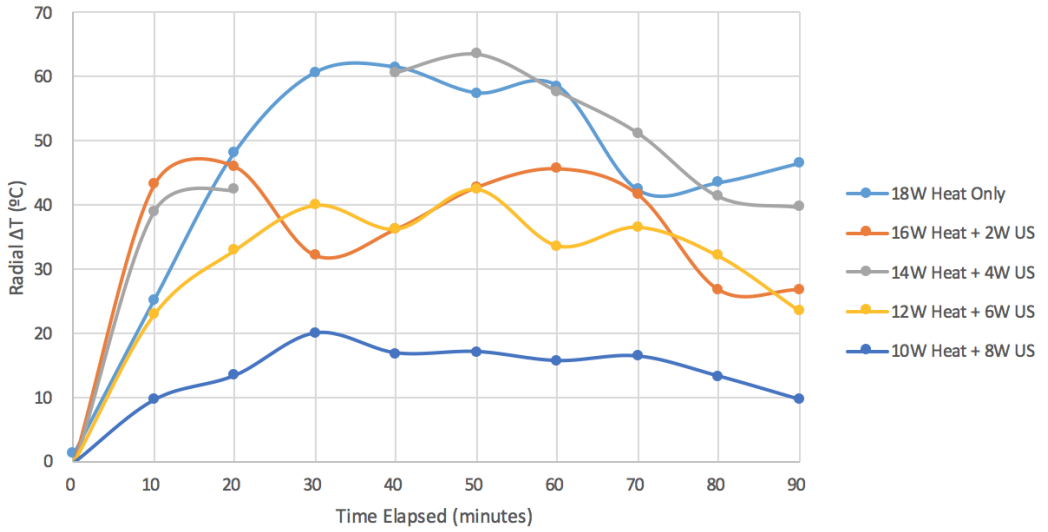

Figure 3.3: Zeolite Temperature Gradient in the Radial Direction of the Desorption Bed

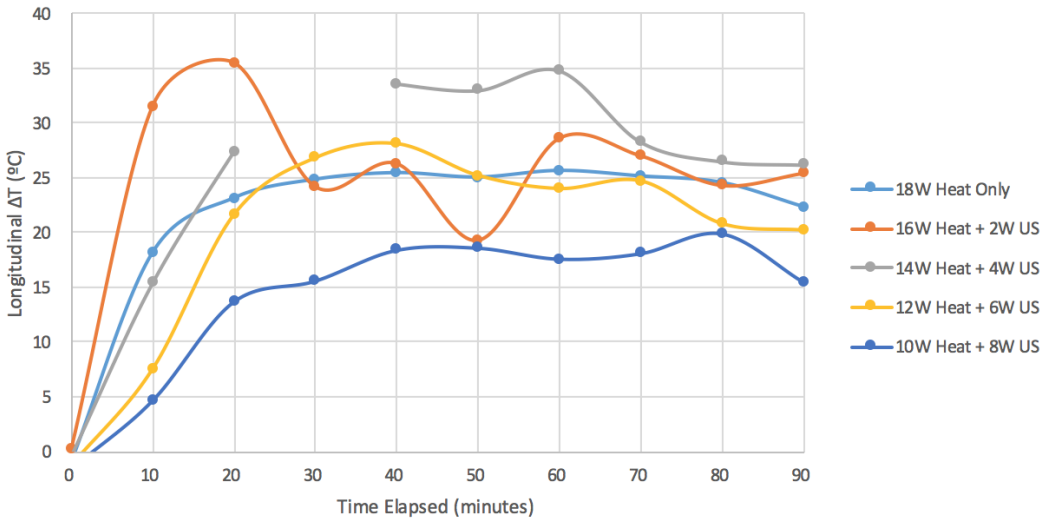

Figure 3.4: Zeolite Temperature Gradient in the Longitudinal Direction of the Desorption Bed

These plots offer excellent insight as to what effect the ultrasound is having on the heat transfer within the bed. Figures 3.1 and 3.2 show pretty consistently that

as the heater power is decreased and the piezoelectric power is increased (keeping the total power into the system at 18W), that the corresponding average temperatures in the radial and longitudinal directions also decrease meaning the ultrasound thermal energy contribution is less than the heating cartridge's, which is to be expected. The behavior appears to be fairly consistent when comparing trials temperature gradient in the radial direction (Figure 3.3), as well. However, when looking at the temperature gradient in the longitudinal direction (Figure 3.4) it can be seen that even as the heater power is decreased, the temperature gradient remains relatively high for the higher heating power trials. Since the lower temperature used in the temperature gradient is the temperature near the bottom of the system, this suggests that the presence of ultrasound assists the conduction of heat towards the top of the bed which may be explained due to heat generation by the ultrasound attenuation.

The temperature results are important to understanding the what is physically occuring within the bed as the result of ultrasound assistance, but the mass change data is more impactful in the context of implementation into a cooling cycle. Here, the metrics defined in section 1.4 will be used to compare how different proportions of heat and ultrasound affect the percent desorbed, the desorption rate, the ultrasonic efficiency, and the total efficiency.

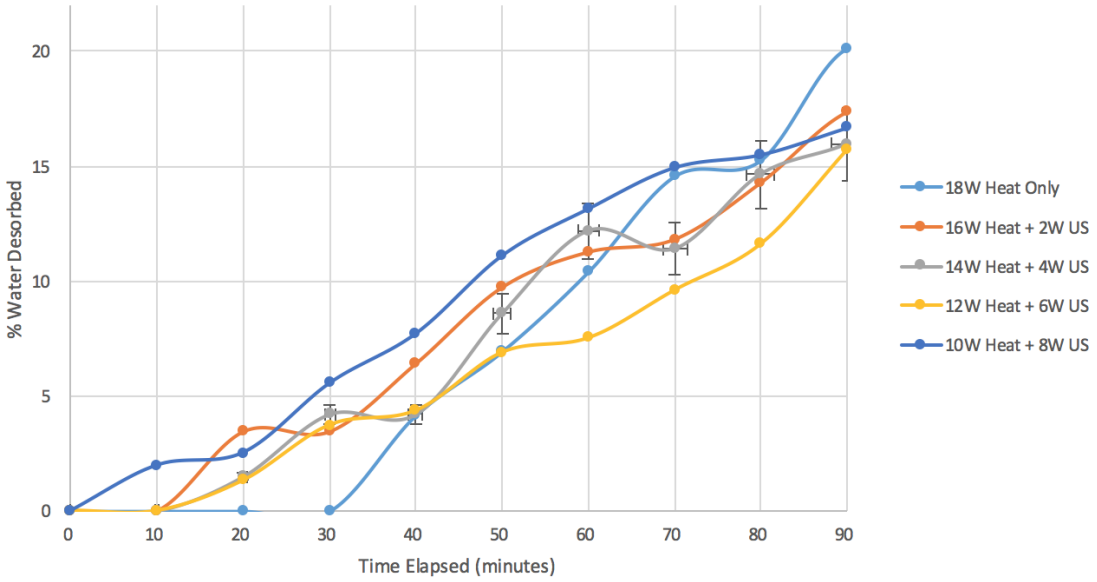

Figure 3.5: Measured Percent Desorbed of Zeolite with varying proportions of Heat and Ultrasound

The cumulative effects of the ultrasound assistance can be seen in Figure 3.5 which accounts for the cumulative desorption that has occured at each time elapsed step. This provides excellent insight as to what effect the ultrasound is having on the desorption process. It is clear that after approximately seventy minutes that the benefit of using ultrasound as opposed to that same magnitude of power in the form of heat diminishes. However, at the beginning of the process, the trials with larger amounts ultrasonic energy show significantly more desorption versus more heat oriented trials. This is highlighted in Figure 3.6.

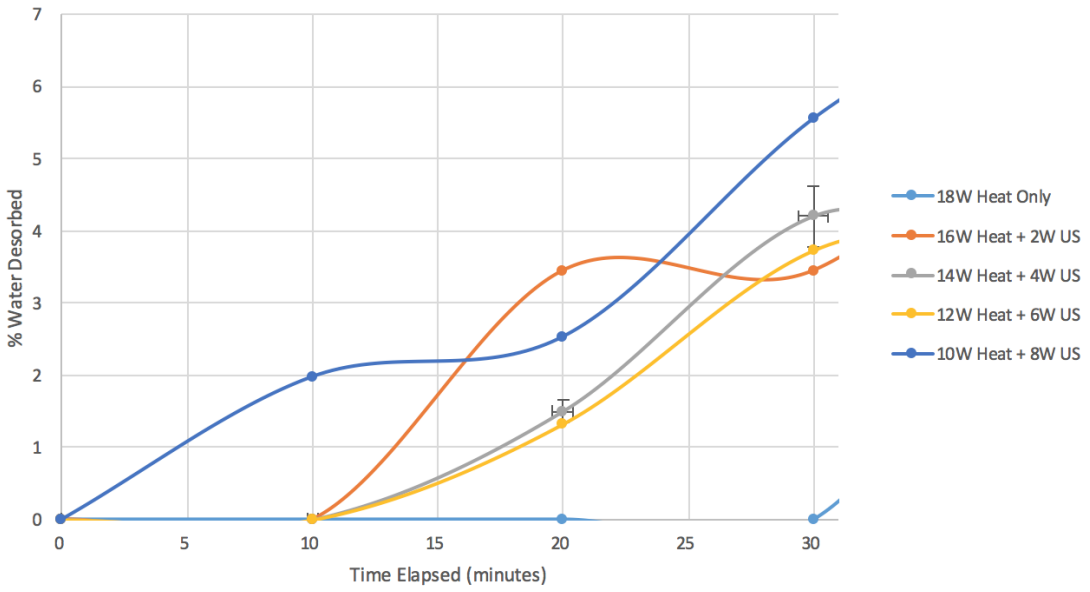

Figure 3.6: Percent Desorption in Zeolite for First Thirty Minutes of All Trials

Based on these results, a case could be made that utilizing ultrasonic energy could help initiate the desorption process, but leveraging that kind of power over heat longer term in the process has diminishing efficiency improvement returns. Additionally examining a time perspective rather than a purely energy one, comparing the amount of time required to achieve five percent desorption can also show the potential of ultrasound enhancement. These times were calculated using the experimental data and linearly interpolating to approximate the time in each trial where the five percent desorption benchmark was achieved. These results are shown in Table 3.1. These results do show a benefit of using ultrasound in the desorption process, but the magnitude of the benefit is inconsistent between trials when comparing this metric.

To use the mass change data in another context, the desorption rate at each timestep is calculated with the results being shown in Figure 3.7. Any reasonable inspection of this data leads to the conclusion that the instantaneous desorption rate is unstable. This is likely due to a wide variety of factors such as the frequent

Table 3.1: Comparison of Time Required to Achieve 5% Desorption by Trial

Trial	Time Required to Achieve 5% Desorption
18W Heat Only	43.0 minutes
16W Heat + 2W US	34.8 minutes
14W Heat + 4W US	41.4 minutes
12W Heat + 6W US	42.5 minutes
10W Heat + 8W US	28.2 minutes

removal of the heater causing the zeolite to shift and the potential for varying moisture concentrations in different parts of the bed. It can also be noted that since there is difference between the definitions for desorption rate and total efficiency (equations 1.3 and 1.6) is several constants, that the total efficiency can be plotted on the same graph as shown on the secondary y-axis. These results show that looking at the results from a cumulative or average perspective rather than instantaneous will provide more insight as to how effective the ultrasound is over the process. A summary of average desorption rate and total efficiency of each trial is shown in table 3.2.

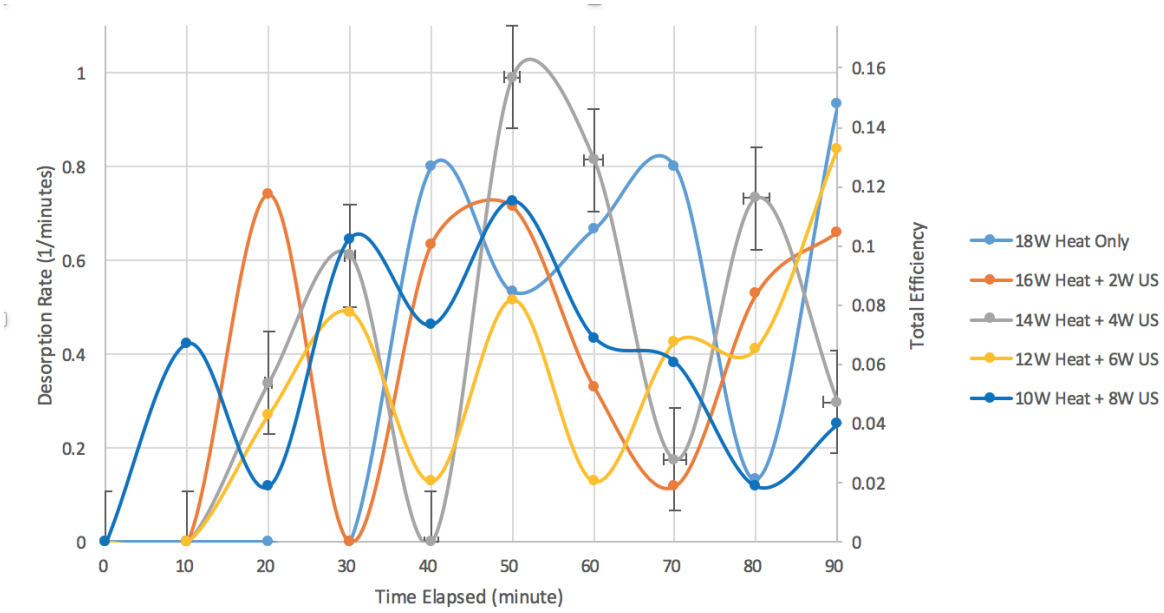

Figure 3.7: Measured Desorption Rate and Total Efficiency of Zeolite with Varying Proportions of Heat and Ultrasound

Table 3.2: Average Desorption Rate and Total Efficiency for Zeolite Trials

	Full Trial		First 30 Minutes	
Trial	AVG DR (1/min)	AVG TE	AVG DR (1/min)	AVG TE
18W Heat Only	0.387	0.061	0	0
16W Heat, 2W US	0.373	0.059	0.247	0.039
14W Heat, 4W US	0.397	0.061	0.317	0.049
12W Heat, 6W US	0.321	0.052	0.254	0.041
10W Heat, 8W US	0.357	0.056	0.396	0.063

These results show that desorption rate and total efficiency are important to understanding the desorption process, but in this context they do not have the sensitivity required to compare trials and a cumulative metric is helps to differentiate which en-

ergy allocation yields the best desorption.

In order to further isolate the effects of both heat and ultrasound, several other trials were completed in which the heat was kept at a constant rate and the power to the piezoelectric was varied as shown in Figure 3.8 and also where the power input to the piezoelectric element was kept constant and the heating power was varied shown in Figure 3.9. What is particularly interesting about these results is the enhancement effect remains throughout the entirety of the trial, rather than just the first portion as seen in the previous trials, granted in these trials the total power input (sum of heat and ultrasound) is not equal, so this is expected to some extent. In particular the 16W of heating power with 6W provided to the piezo is shows excellent results which indicate that there may be a threshold value of the sum of power input in which ultrasound becomes more effective.

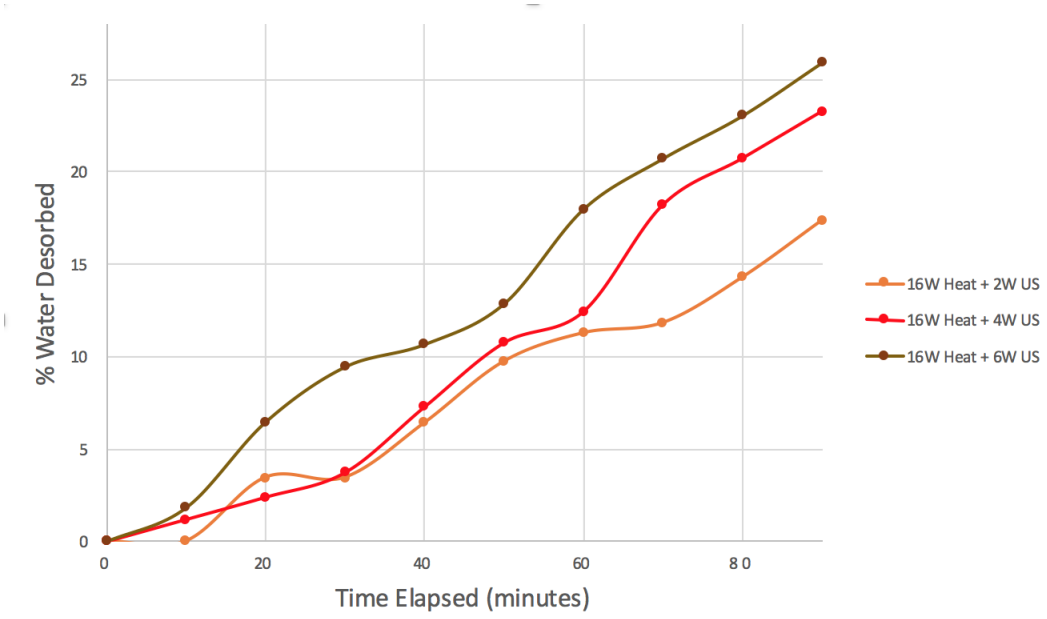

Figure 3.8: Zeolite Percent Desorbed for Constant Heat, Variable Power Input to Piezoelectric

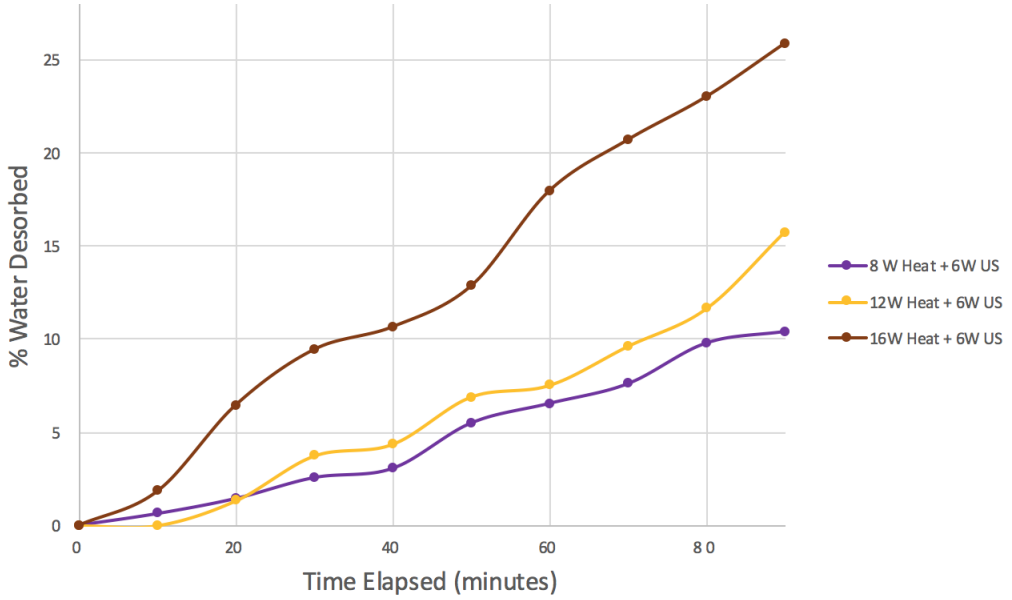

Figure 3.9: Zeolite Percent Desorbed for Constant Input Power to Piezoelectric, Variable Heat

Finally, experimental results for the ultrasonic efficiency can be presented. Recall ultrasonic efficiency was defined in equation 1.5 and that this metric quantifies the impact of the ultrasonic energy provided. To interpret this metric appropriately, the heating provided must be constant and the ultrasonic energy must be varied as previously seen in Figure 3.8. Thus, the positive impact on the desorption process that the ultrasound provides is further seen in Figure 3.10.

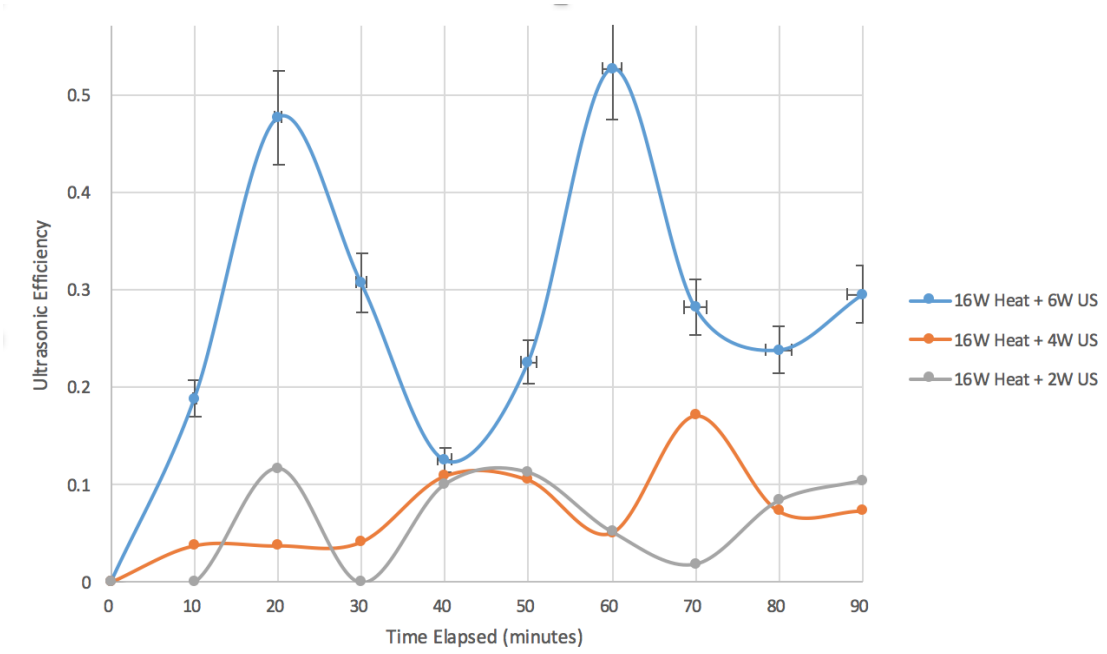

Figure 3.10: Ultrasonic Efficiency in zeolite for Several Trials with Constant Heat Input

Figure 3.10 further suggests that there may be a threshold power amount input to the system where the enhancement effect of the ultrasound becomes more pronounced. Further trials at higher heating and ultrasound inputs could better characterize this behavior.

3.2 Sodium Polyacrylate

Using the same methodology as presented in the zeolite trials, the temperature results for the sodium polyacrylate trials can be plotted in the same way. However, working with sodium polyacrylate did amplify some of the issues observed in the zeolite trials. Most importantly, very limited temperature data for trials using ultrasound was able to be acquired. This is due to the much less electrically insulative properties of the sodium polyacylate (in comparison to zeolite) which did not shield

the thermocouples and DAQ from significant electrical signals. For this reason, of the two completed sodium polyacrylate trials completed with ultrasound, only one hour of temperature data from one trial was able to be obtained. It is also worth noting at this moment that these trials are do not sum to the same amount of energy as was done with zeolite and that unlike the zeolite trials the catridge heater was not removed to take mass measurements due to a smaller heater being employed and the coupling between the heater and the bed being less rigid. The resulting plots for the previously discussed metrics are shown below in Figures 3.11-3.14.

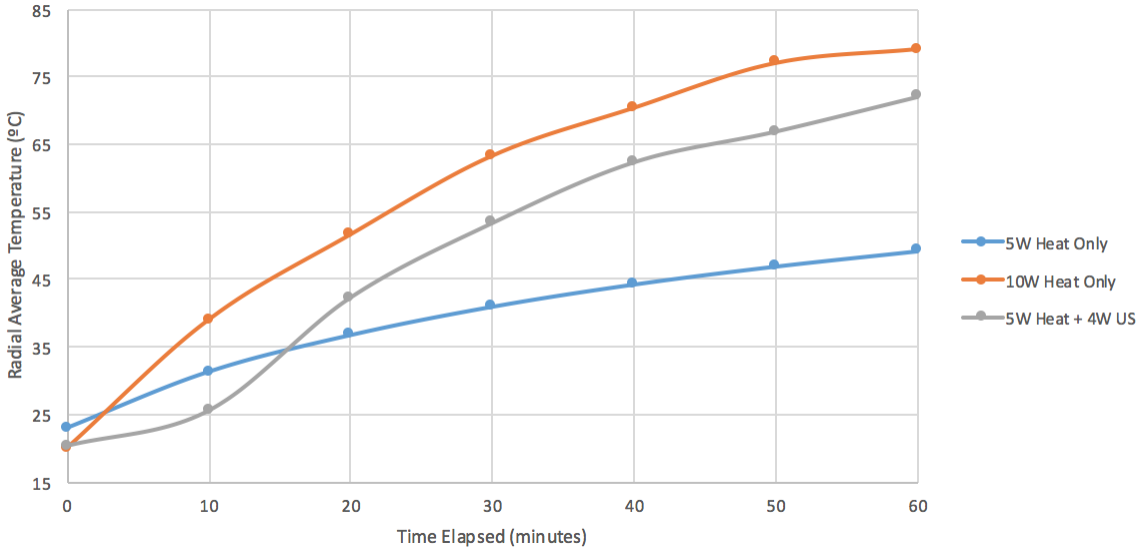

Figure 3.11: Sodium Polyacrylate Average Temperature in the Radial Direction of the Desorption Bed

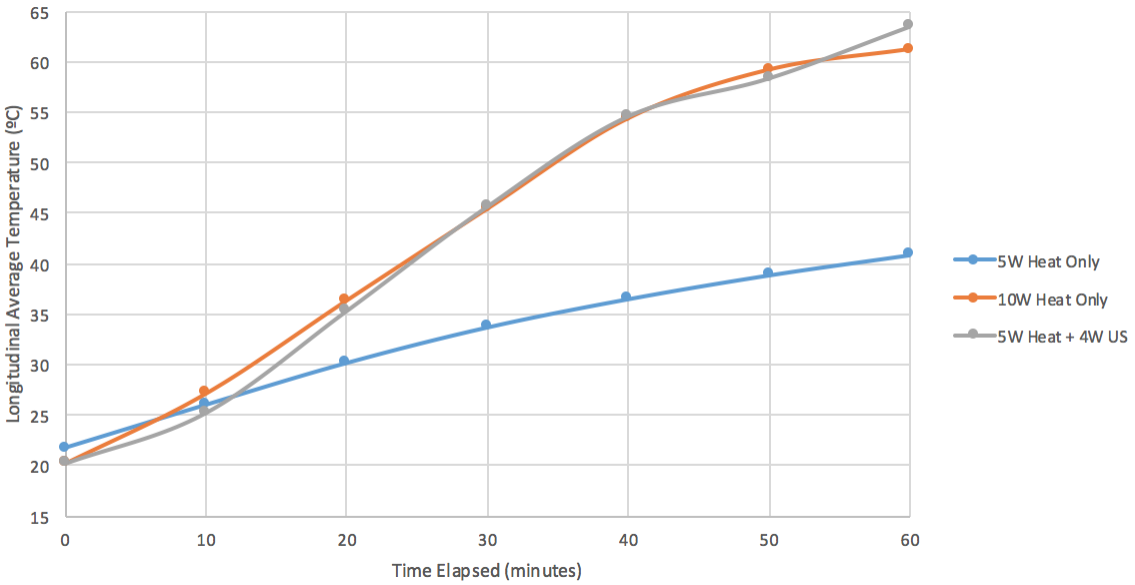

Figure 3.12: Sodium Polyacrylate Average Temperature in the Longitudinal Direction of the Desorption Bed

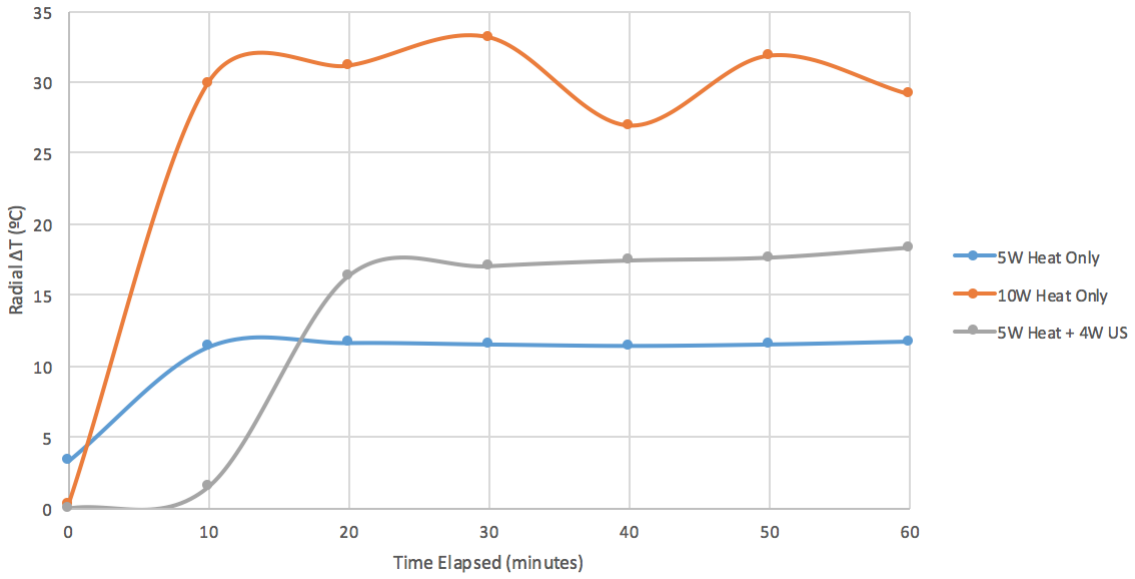

Figure 3.13: Sodium Polyacrylate Temperature Gradient in the Radial Direction of the Desorption Bed

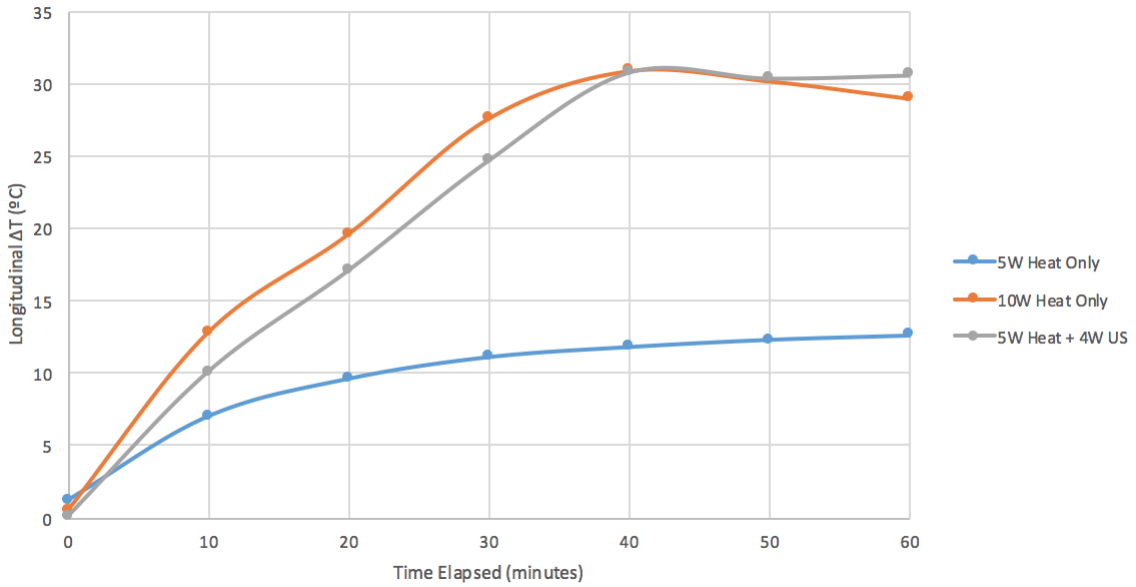

Figure 3.14: Sodium Polyacrylate Temperature Gradient in the Longitudinal Direction of the Desorption Bed

Even with this limited data, some pretty interesting observations can be made. The average temperatures shown in Figures 3.11 and 3.12, show that the even though the heating power is half between the 10W heat only and the 5W heat plus 4W ultrasound trial, that their average temperatures are surprisingly well matched. Furthermore, it can be seen in Figure 3.13 that the temperature gradient is consistently and significantly smaller in the ultrasound trial. What this means is that the heat is far more evening distributed in the ultrasound trial versus the heat only trial. This could in part be explained by the fact that the piezo itelf generates heat as it is being powered, but that alone likely is not enough to cause the significant shift in the radial thermal gradient. This suggests that the ultrasound itself is helping to promote heat transfer within the bed.

Now, the desorption data can be presented much in a similar way as was done for the zeolite trials. The resulting plots are shown in Figures 3.15 and 3.16 .

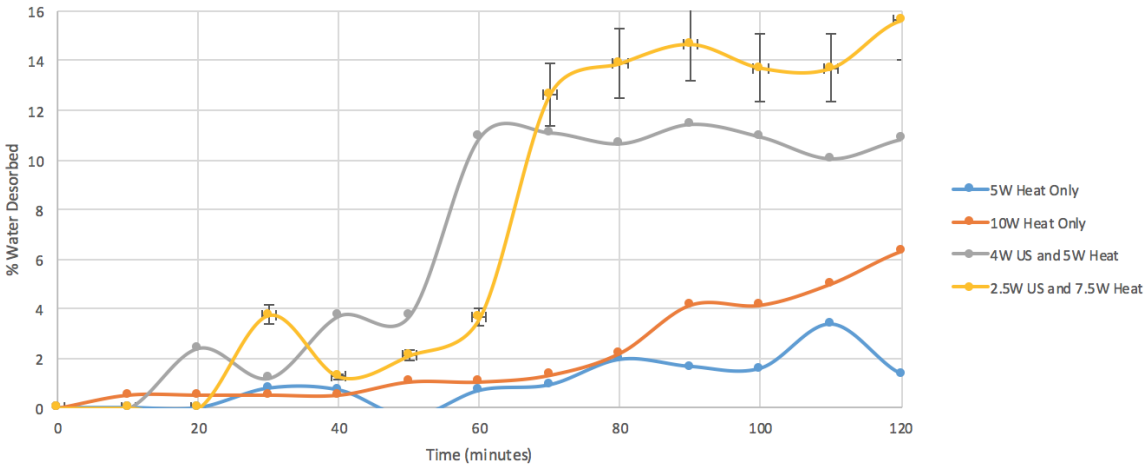

Figure 3.15: Measured Percent Desorbed of Sodium Polyacrylate with varying proportions of Heat and Ultrasound

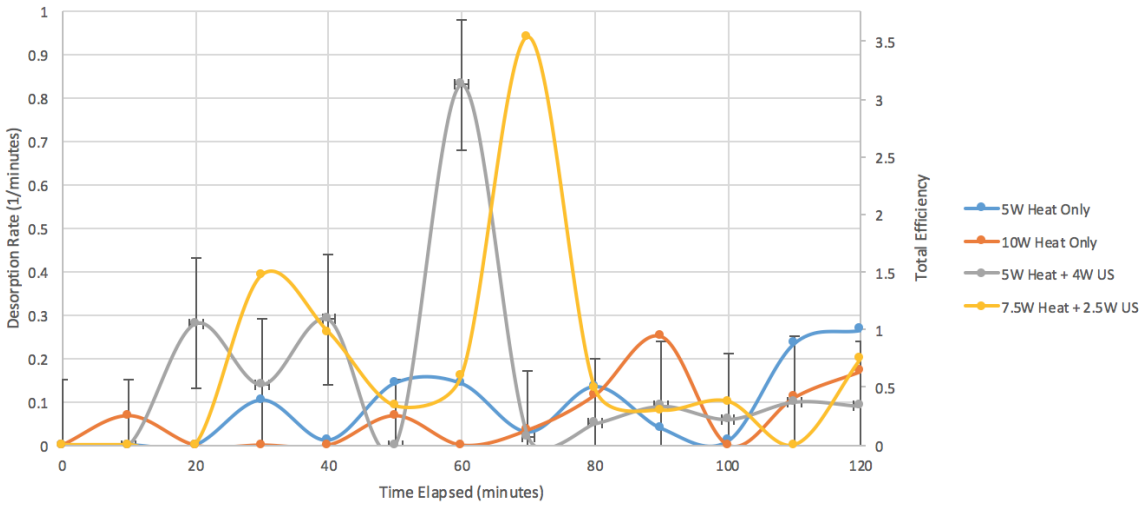

Figure 3.16: Measured Desorption Rate and Total Efficiency of Sodium Polyacrylate with Varying Proportions of Heat and Ultrasound

Figure 3.16 shows again that the desorption rate is not stable for this material and again showing that a more cumulative metric would be more enlightening to review. Figure 3.15 does show the long term trend of each trial with some promising results.

The most significant aspect of Figure 3.15 to notice is the large spike in desorption (also visible in Figure 3.16) at around the one hour mark for trials with ultrasound. Without this spike, the sodium polyacrylate performs roughly as well as the heat only trials, but with the spike the overall desorption for the trial is two to three times higher. There is currently not a good model to explain why this sharp increase in desorption is seen at this time in both ultrasound trials and more investigation will be required.

Unfortunately, after the second trial with ultrasound the piezoelectric element appears to have burned out and is no longer usable. This presents additional inconvenience in that in order to make the bed liquid-tight, all wired components (including the piezo) needed to have their wires epoxied into the holes in the bed making the piezoelectric non-removable. This suggests that going forward a different design be used such that the piezoelectric is not in direct contact with the essentially liquid water sodium polyacrylate which is suspect in the piezo's early failure.

Chapter 4

CONCLUSIONS AND FUTURE WORK

Based on the results presented in the previous section, conclusions as to the effect of using ultrasound to enhance the desorption process can be made. There were more zeolite trials and the results prove to be more conclusive that using ultrasound to supplement heat greatly enhances the initiation of the desorption process. Based on the data presented, this benefit appears to be less significant as time goes on meaning that using ultrasound for the entirety of desorption may not be as efficient as just employing it at the beginning of the process and then tapering it off. Novel designs for such a system may prove to be more effective the currently available adsorption cooling systems.

There is a clear benefit to utilizing ultrasound in the desorption process in sodium polyacrylate, as well. There are practical considerations that must be resolved such as the effect of direct contact with the piezoelectric element before long-term viability can be achieved, but there is much potential. It is unfortunate that more trials were not able to be completed before the conclusion of this study and further investigation as to why there is a repeatable spike in the desorption at a certain point in the process. Understanding this large increase in the desorption rate may be the key to making this material usable in cooling applications.

Future work for both of these materials would be extremely beneficial to develop a more fundamental understanding of what is physically occuring in the desorption bed. For zeolite, using a different material to construct the bed would enable higher heating power to be used without the risk of melting the bed and higher power investigations may show ultrasounds benefit increases at higher powers. For sodium

polyacrylate, there is significant potential in this material if the piezoelectric and sorbent can be used not in direct contact with one another. This would prolong the life of the piezoelectric and bed and allow a more sustainable experimental set-up to be used. A future study could include both microscopic and infared observations to visualize how exactly the desorption process occurs when subject to ultrasound would be extremely helpful in designing internal bed geometry to optimize desorption.

Additional future work could include redesigning the bed to allow the mechanical waves generated by the piezoelectric to be transmitted more uniformly to the sorbent. In this study, direct contact between the piezoelectric and sorbent was made, but since the sorbent is not a continuous solid material there is decay in the intensity of the wave as it has to be transmitted between unrestrained sorbent and air gaps. Further improvements to this system could be observed if as much of the sorbent as possible is in direct contact with the ultrasound generator, rather than a small portion. This could be done by coupling a attenuating material in the form of a grid to the piezoelectric allowing for more wave propagation to the sorbent.

Finally, further future work should include computer simulations to see if further understanding could be achieved from a numerical model. COMSOL®contains a suite of softwares built for just such an analysis and a model using this software is currently being developed. Such a model can be validated using current and future experimental data and provide a more fundamental picture of how the desorption process is being effected by the ultrasonic power provided.

REFERENCES

[1] Ruren Xu, Wenqin Pang, Jihong Yu, Huo Qisheng, and Jiesheng Chen. *Chemistry of Zeolites and Related Porous Materials*. John Wiley Sons Ltd., Hoboken, New Jersey, 2007.

[2] Lenntech BV. Zeolites-applications, 2018. URL https://www.lenntech.com/library/media-filtration/zeolites-applications.htm.

[3] Wikimedia Commons. Zeolite, 2016. URL https://commons.wikimedia.org/wiki/File:Zeolite-ZSM-5-3D-vdW.png.

[4] The Royal Society of Chemistry. Chemists pore over zeolite and watch holes open up, 2016. URL https://www.chemistryworld.com/news/chemists-pore-over-zeolites-and-watch-holes-open-up/2500166.article.

[5] Juan A. Gallego-Juarez and Karl. Graff. *Power Ultrasonics: Applications of High-Intensity Ultrasound*. Woodhead Publishing, Sawston, Cambridge, UK, 2014.

[6] Materials RECYCphp and Solutions. Super absorbent sodium polyacrylate manufacturer, 2018. URL http://recycphp.com/en/p/materials/sodium-polyacrylate/.

[7] Open Chemistry Database PubChem. Sodium polyacrylate, 2018. URL https://pubchem.ncbi.nlm.nih.gov/compound/sodium_acrylate#section=Information-Sources.

[8] Robert Fiero. Polymers-osmosis magic, 2015. URL https://sites.google.com/site/sed695b3/projects/discrepant-events/osmosis-magic.

[9] Hasan Demir. Experimental study on a novel microwave-assisted adsorption heat pump. *International Journal of Refrigeration*, 45:35–43, 2014.

[10] Hasan Demir. Development of microwave assisted zeolite-water adsorption heat pump. *International Journal of Refrigeration*, 36:2289–2296, 2013.

[11] Ye Yao, Weijiang Zhang, and Shiqing Liu. Parametric study of high-intensity ultrasonics for silica gel regeneration. *Energy and Fuels*, 23:3150–3158, 2009.

[12] Ye Yao, Weijiang Zhang, and Shiqing Liu. Regeneration of silica gel using high-intensity ultrasonic under low temperatures. *Energy and Fuels*, 23:457–463, 2009.

[13] K. Oertel and M. Fischer. Adsorption cooling system for cold storage using methanol/silica gel. *Applied Thermal Engineering*, 18:773–786, 1998.

[14] Michael J. Moran, Howard N. Shapiro, Bruce R. Munson, and David P. DeWitt. *Introduction to Thermal Systems Engineering*. John Wiley Sons Ltd., Hoboken, New Jersey, 2003.

[15] Tydex Research and Industrial Optics. Thz materials, 2018. URL http://www.tydexoptics.com/products/thz_optics/thz_materials/.

[16] Theodore L. Brown, Eugene H. LeMay, Bruce E. Bursten, Catherine J. Murphy, and Patric Woodward. *Chemistry: The Central Science*. Pearson-Prentice Hall, Upper Saddle River, New Jersey, 2009.

[17] Ltd. APC International. Physical and piezoelectric properties of apc materials, 2018. URL https://www.americanpiezo.com/apc-materials/physical-piezoelectric-properties.html.

[18] Stewart Sherrit and Binu K. Mukherjee. Characterization of piezoelectric materials for transducers. Technical report, Jet Propulsion Laboratory, California Institute of Technology, Pasadena, California, USA, 2007.

[19] Mikio Umeda, Kentaro Nakamura, and Sadayuki Ueha. The measurment of high-power characteristics for a piezoelectric transducer based on the electrical transient response. *Japanese Journal of Applied Physics*, 37:5322–5325, 1998.

[20] Thomas G. Beckwith and Roy D. Marangoni. *Mechanical Measurements*. Addison-Wesley Publishing Company, Reading, Massachusetts, 1990.

[21] Sigma-Aldrich. Molecular sieves - technical information bulletin, 2018. URL https://www.sigmaaldrich.com/chemistry/chemical-synthesis/learning-center/technical-bulletins/al-1430/molecular-sieves.html.

[22] IMPAK Corporation. Desiccant chart comparisons, 2018. URL https://www.sorbentsystems.com/desiccants_charts.html.

APPENDIX A

ZEOLITE DESORPTION DATA COLLECTED FEBRUARY-MARCH 2018

18W Heat Only

t (min)	mass (g)	Mass of zeolite (g)	Mass desorbed (g)	%desorbed
0	258.9	81.7	0	0.00
10	258.9	81.7	0	0.00
20	258.9	81.7	0	0.00
30	258.9	81.7	0	0.00
40	258.3	81.1	0.6	4.16
50	257.9	80.7	1	6.93
60	257.4	80.2	1.5	10.40
70	256.8	79.6	2.1	14.56
80	256.7	79.5	2.2	15.25
90	256	78.8	2.9	20.10

DR (1/min)	TE
0.00	0.00
0.00	0.00
0.00	0.00
0.00	0.00
0.80	0.13
0.53	0.08
0.67	0.10
0.80	0.13
0.13	0.02
0.93	0.15

16W Heat + 2W US

t (min)	mass (g)	Mass of zeolite (g)	Mass desorbed (g)	%desorbed
0	259.92	81.16	0.00	0.00
10	259.92	81.16	0.00	0.00
20	259.36	80.6	0.56	3.45
30	259.36	80.6	0.56	3.45
40	258.88	80.12	1.04	6.41
50	258.34	79.58	1.58	9.73
60	258.09	79.33	1.83	11.27
70	258	79.24	1.92	11.83
80	257.6	78.84	2.32	14.29
90	257.1	78.34	2.82	17.37

DR (1/min)	UE	TE
0.00	0.00	0.00
0.00	0.00	0.00
0.74	1.05	0.12
0.00	0.00	0.00
0.64	0.90	0.10
0.72	1.02	0.11
0.33	0.47	0.05
0.12	0.17	0.02
0.53	0.75	0.08
0.66	0.94	0.10

14W Heat + 4W US

t (min)	mass (g)	Mass of zeolite (g)	Mass desorbed (g)	%desorbed
0	263.6	83.25	0	0.00
10	263.6	83.25	0	0.00
20	263.35	83	0.25	1.50
30	262.9	82.55	0.7	4.20
40	262.9	82.55	0.7	4.20
50	262.17	81.82	1.43	8.59
60	261.57	81.22	2.03	12.19
70	261.7	81.35	1.9	11.41
80	261.16	80.81	2.44	14.65
90	260.94	80.59	2.66	15.98

DR (1/min)	TE
0.00	0.00
0.00	0.00
0.34	0.05
0.61	0.09
0.00	0.00
0.99	0.15
0.82	0.13
0.18	0.03
0.73	0.11
0.30	0.05

12W Heat + 6W US

t (min)	mass (g)	Mass of zeolite (g)	Mass desorbed (g)	%desorbed
0	259.79	79.09	0	0.00
10	259.79	79.09	0	0.00
20	259.58	78.88	0.21	1.33
30	259.2	78.5	0.59	3.73
40	259.1	78.4	0.69	4.36
50	258.7	78	1.09	6.89
60	258.6	77.9	1.19	7.52
70	258.27	77.57	1.52	9.61
80	257.95	77.25	1.84	11.63
90	257.3	76.6	2.49	15.74

DR (1/min)	TE
0.00	0.00
0.00	0.00
0.27	0.04
0.49	0.08
0.13	0.02
0.52	0.08
0.13	0.02
0.43	0.07
0.41	0.07
0.84	0.14

10W Heat + 8W US

t (min)	mass (g)	Mass of zeolite (g)	Mass desorbed (g)	%desorbed
0	261.6	80.98	0	0.00
10	261.28	80.66	0.32	1.98
20	261.19	80.57	0.41	2.53
30	260.7	80.08	0.9	5.56
40	260.35	79.73	1.25	7.72
50	259.8	79.18	1.8	11.11
60	259.47	78.85	2.13	13.15
70	259.18	78.56	2.42	14.94
80	259.09	78.47	2.51	15.50
90	258.9	78.28	2.7	16.67

DR (1/min)	TE
0.00	0.00
0.42	0.07
0.12	0.02
0.65	0.10
0.46	0.07
0.73	0.11
0.44	0.07
0.38	0.06
0.12	0.02
0.25	0.04

16W Heat + 6W US

t (min)	mass (g)	Mass of zeolite (g)	Mass desorbed (g)	%desorbed
0	262.3	82.04	0	0.00
10	262	81.74	0.3	1.83
20	261.24	80.98	1.06	6.46
30	260.75	80.49	1.55	9.45
40	260.55	80.29	1.75	10.67
50	260.19	79.93	2.11	12.86
60	259.35	79.09	2.95	17.98
70	258.9	78.64	3.4	20.72
80	258.52	78.26	3.78	23.04
90	258.05	77.79	4.25	25.90

DR (1/min)	UE	TE
0.00	0.00	0.00
0.40	0.19	0.05
1.02	0.48	0.13
0.66	0.31	0.08
0.27	0.13	0.03
0.48	0.23	0.06
1.12	0.53	0.14
0.60	0.28	0.08
0.51	0.24	0.07
0.63	0.29	0.08

8W Heat + 6W US

t (min)	mass (g)	Mass of zeolite (g)	Mass desorbed (g)	%desorbed
0	260	80.1	0	0.00
10	259.9	80	0.1	0.62
20	259.77	79.87	0.23	1.44
30	259.59	79.69	0.41	2.56
40	259.51	79.61	0.49	3.06
50	259.12	79.22	0.88	5.49
60	258.95	79.05	1.05	6.55
70	258.78	78.88	1.22	7.62
80	258.43	78.53	1.57	9.80
90	258.33	78.43	1.67	10.42

DR (1/min)	TE
0.00	0.00
0.13	0.03
0.17	0.03
0.24	0.05
0.10	0.02
0.51	0.10
0.22	0.05
0.22	0.05
0.46	0.09
0.13	0.03

16W Heat + 4W US

t (min)	mass (g)	Mass of zeolite (g)	Mass desorbed (g)	%desorbed
0	263.2	83.7	0	0.00
10	263	83.5	0.2	1.20
20	262.8	83.3	0.4	2.40
30	262.58	83.08	0.62	3.73
40	262	82.5	1.2	7.27
50	261.44	81.94	1.76	10.74
60	261.17	81.67	2.03	12.43
70	260.26	80.76	2.94	18.20
80	259.87	80.37	3.33	20.72
90	259.48	79.98	3.72	23.26

DR (1/min)	UE	TE
0.00	0.00	0.00
0.27	0.19	0.04
0.27	0.19	0.04
0.30	0.21	0.04
0.79	0.55	0.11
0.76	0.53	0.11
0.37	0.25	0.05
1.24	0.86	0.17
0.53	0.37	0.07
0.53	0.37	0.07

APPENDIX B

SODIUM POLYACRYLATE DESORPTION DATA COLLECTED FEBRUARY 2018

5W Heat only

Time (minutes)	Total Mass (g)	Portion of mass loss	Percent desorbed	DR (1/min)
0	283.3	1.00	0.00	0.00
10	283.3	1.00	0.00	0.00
20	283.3	1.00	0.00	0.00
30	282.26	0.99	0.79	0.10
40	282.37	0.99	0.70	0.01
50	283.8	1.00	-0.38	0.14
60	282.38	0.99	0.70	0.14
70	282.08	0.99	0.92	0.03
80	280.73	0.98	1.95	0.13
90	281.11	0.98	1.66	0.04
100	281.2	0.98	1.59	0.01
110	278.85	0.97	3.37	0.23
120	281.5	0.99	1.36	0.26

10W Heat Only

Time (minutes)	Total Mass (g)	Portion of mass loss	Percent Desorbed
0	291.36	1.00	0.00
10	290.68	0.99	0.53
20	290.68	0.99	0.53
30	290.68	0.99	0.53
40	290.68	0.99	0.53
50	290	0.99	1.05
60	290	0.99	1.05
70	289.65	0.99	1.32
80	288.5	0.98	2.21
90	286	0.96	4.14
100	286	0.96	4.14
110	284.9	0.95	4.99
120	283.2	0.94	6.31

DR (1/min)
0.00
0.07
0.00
0.00
0.00
0.07
0.00
0.04
0.11
0.25
0.00
0.11
0.17

4W US and 5W Heat

Time (minutes)	Total Mass (g)	Portion of mass loss	Percent desorbed
0	272.9	1.00	0.00
10	272.9	1.00	0.00
20	270.1	0.98	2.43
30	271.5	0.99	1.22
40	268.6	0.96	3.73
50	268.6	0.96	3.73
60	260.3	0.89	10.94
70	260.1	0.89	11.12
80	260.6	0.89	10.68
90	259.7	0.89	11.46
100	260.3	0.89	10.94
110	261.3	0.90	10.07
120	260.4	0.89	10.86
130	260	0.89	11.20

DR (1/min)
0.00
0.00
0.28
0.14
0.29
0.00
0.83
0.02
0.05
0.09
0.06
0.10
0.09
0.04

2.5W US and 7.5W Heat

Time (minutes)	Total Mass (g)	Portion of mass loss	Percent desorbed
0	262.21	1.00	0.00
10	262.21	1.00	0.00
20	262.21	1.00	0.00
30	258.3	0.96	3.74
40	260.9	0.99	1.25
50	260	0.98	2.12
60	258.4	0.96	3.65
70	249	0.87	12.65
80	247.7	0.86	13.90
90	246.9	0.85	14.66
100	247.9	0.86	13.71
110	247.9	0.86	13.71
120	245.9	0.84	15.62

DR (1/min)	TE
0.00	0.00
0.00	0.00
0.00	0.00
0.39	1.47
0.26	0.98
0.09	0.34
0.16	0.60
0.94	3.54
0.13	0.49
0.08	0.30
0.10	0.38
0.00	0.00
0.20	0.75

APPENDIX C

ZEOLITE TEMPERATURE DATA COLLECTED FEBRUARY-MARCH 2018

18W Heat Only

Time (min)	T1 AVG (C)	T2 AVG (C)	T3 AVG (C)	T4 AVG (C)
0	21.1	20.6	20.8	20.7
10	23.5	43.2	42	39.2
20	24.6	63.7	62.3	61.5
30	24.8	75.5	77	78.9
40	25.5	83.9	85.2	86.3
50	25.8	86.5	87.9	90.1
60	25.5	90.2	90.4	90.8
70	25.9	90.9	91.2	91.8
80	26	91.2	91.3	91.6
90	26.9	92.5	94.3	96.3

T5 AVG (C)	T6 AVG (C)	T7 AVG (C)
21.6	21.4	20.2
25.1	48.2	23
40.6	88.7	40.5
50.7	120.8	60.2
58.5	135.6	74.2
61.5	143.4	86
64.6	152.6	94.1
65.8	147.9	105.6
66.7	156	112.6
70.2	162.4	116

16W Heat + 2W US

Time (min)	T1 AVG (C)	T2 AVG (C)	T3 AVG (C)	T4 AVG (C)
0	23	22.5	23	23.7
10	25.4	63	61.6	50.8
20	25.9	81.8	84.6	70.1
30	25.5	78.7	85.2	76.2
40	25.6	88.8	96.8	90.6
50	25.8	89.9	105.5	104.9
60	26	105.6	115.1	108.7
70	26.5	108.5	116.2	114.9
80	26	107.6	117.4	115.7
90	25.9	111.4	120.7	116.7

T5 AVG (C)	T6 AVG (C)	T7 AVG (C)
22.3	21.9	22.3
31.5	73.1	30
46.3	93.1	47.2
54.5	91.1	59
62.5	106.4	70.2
70.6	120.9	78.2
77	129.8	84.2
81.5	132.9	91.3
83.3	124	97.2
86	130.3	103.5

14W Heat + 4W US

Time (min)	T1 AVG (C)	T2 AVG (C)	T3 AVG (C)	T4 AVG (C)
0	23.6	21.1	21.4	21.3
10	24.4	47.2	47	47.8
20	24.4	73.6	70.9	67.3
30				
40	21.4	107.2	109.7	
50	24.3	114.1	118.3	
60	26.8	118.2	124.8	120.2
70	26.3	114.5	120.7	120.8
80	26.5	112.8	116.8	119
90	36.8	115	115.6	117.3

T5 AVG (C)	T6 AVG (C)	T7 AVG (C)
21.5	19.9	20.9
31.8	66	27
46.2	82.1	39.8
73.6	125.3	64.7
81.1	135.5	72
83.4	135.9	78.2
86.2	133.8	82.6
86.3	129.7	88.4
88.8	133.2	93.6

12W Heat + 6W US

Time (min)	T1 AVG (C)	T2 AVG (C)	T3 AVG (C)	T4 AVG (C)
0	25	21.2	22.15	22.4
10	25	47.5	42.8	40.6
20	25.3	69.7	63.8	60.4
30	25.7	83.5	75.3	72.2
40	28.1	91.6	84.8	81.9
50	26.6	92.3	86.7	85.3
60	28.8	94.6	90.5	88.9
70	36.3	95.6	91.1	89.5
80	27.1	95.2	93.1	91.9
90	28	95.5	93.6	92.3

T5 AVG (C)	T6 AVG (C)	T7 AVG (C)
22.5	22.5	22.7
40	53.4	30.5
48.1	77.6	44.7
56.7	97.6	57.7
63.5	106.2	70
67.1	115.1	72.7
70.6	111.1	77.5
70.9	117.7	81.2
74.4	117	85
75.3	114.4	90.9

10W Heat + 8W US

Time (min)	T1 AVG (C)	T2 AVG (C)	T3 AVG (C)	T4 AVG (C)
0	24.5	20.5	21.5	21.5
10	24.5	34.4	33.7	32.5
20	25.1	50.9	47.9	44.9
30	25.4	61.7	59.3	57.4
40	25.9	70.7	67.3	65
50	26.1	75	72.5	70
60	26.1	78.6	76.5	75.7
70	26.7	81.1	81	77.9
80	25.9	83.6	80	78.2
90	25.8	80	80.1	79.1

T5 AVG (C)	T6 AVG (C)	T7 AVG (C)
22	20.5	20.8
29.7	42.2	32.7
37.2	60.5	47.2
46.1	77.2	57.3
52.3	81.7	64.9
56.4	89.1	72.1
61	92.9	77.3
63	97.7	81.4
63.7	96	82.8
64.5	91.8	82.2

16W Heat + 6W US

Time (min)	T1 AVG (C)	T2 AVG (C)	T3 AVG (C)	T4 AVG (C)
0	23.4	21.3	22	22.7
10	25.1	49.4	44.6	41.2
20	25.8	74.1	67.4	63.3
30	26.3	87.1	83.5	80.2
40	26.2	96.9	91.1	89
50	26.4	96.5	95.7	92.1
60	26.9	107	102.5	100.1
70	26.7	113.2	106.7	106
80	26.8	116.3	108.3	107.6
90	26.7	117.2	112	114.7

T5 AVG (C)	T6 AVG (C)	T7 AVG (C)
20.8	20.6	21.7
32.5	64.6	41.4
47.5	87.7	62.8
60.2	109.2	78.1
66.7	114	91.6
70.4	117	96.2
75.3	134	103.8
79.9	138.9	106.8
81.4	136.3	110.5
85.9	137	111.5

8W Heat + 6W US

Time (min)	T1 AVG (C)	T2 AVG (C)	T3 AVG (C)	T4 AVG (C)
0	23.6	21.2	21.6	21.5
10	24.9	33.3	31.8	32
20	25.3	45.6	42.8	42.4
30	27.6	56.7	53.5	53.1
40	27.8	61	59.5	58.7
50	27.1	68	63.6	63.1
60	26.9	69.8	67.3	65.7
70	27.4	68.7	67.9	68.1
80	28	69.3	68.4	69.6
90	26.9	71.4	71.3	72.9

T5 AVG (C)	T6 AVG (C)	T7 AVG (C)
22.9	21	21.8
30	45.6	33
37.1	61.5	42.8
42.7	71	50
48.3	75.8	61.6
51.9	76.9	66.2
53.8	88	67.7
55.5	87.2	68.4
56.7	90.6	71.7
58.5	96.6	71.6

16W Heat + 4W US

Time (min)	T1 AVG (C)	T2 AVG (C)	T3 AVG (C)	T4 AVG (C)
0	26.3	23.5	24.6	24.6
10	26.7	47.7	44.2	42.6
20	26.7	63.1	58.5	57.1
30	26.9	78.7	75.6	76.8
40	26.9	86.4	81.9	83.9
50	26.6	95.3	88.2	89.5
60	26.9	102.9	96.2	99.8
70	27.4	105	103	104.4
80	26.7	106.2	106.8	109.3
90	26.8	108.9	109.5	115.4

T5 AVG (C)	T6 AVG (C)	T7 AVG (C)
25.2	23	24.6
32.3	52.4	37.2
42.8	86.7	59.6
53.9	101.3	71.3
59.7	122.8	81.2
65.8	136.3	96.2
72.6	135.9	101.9
76.6	133.5	109.1
80.3	152.7	106.8
84.7	154.1	108.3

APPENDIX D

SODIUM POLYACRYLATE TEMPERATURE DATA COLLECTED FEBRUARY 2018

5W Heat Only

Time (min)	T1 AVG (C)	T2 AVG (C)	T3 AVG (C)	T4 AVG (C)
0	21.2	21.6	22	22.4
10	23	25.7	27.7	30
20	25.8	29.8	32.5	35.4
30	28.6	33.3	36.6	39.7
40	31.1	36.4	39.7	42.9
50	33.3	38.9	42.3	45.6
60	35.2	41.1	44.6	47.8
70	37	43.2	46.7	49.8
80	38	44.4	48	51.6
90	39.4	45.8	49.4	53.1
100	40.6	47	50.7	54.6
110	41.2	47.9	51.8	55.5
120	41.9	48.8	52.7	56.5

T5 AVG (C)	T6 AVG (C)	T7 AVG (C)
21.6	24.9	21.6
23.7	37.6	26.3
27.3	43.2	31.6
30.2	47.3	35.8
32.3	50.6	39.2
34.1	53.3	41.8
35.5	55.7	44
37.1	57.9	46.2
38.4	60.1	47.8
39.6	61.8	49.3
41.2	63.1	50.7
41.3	63.7	51.6
41.8	64.7	52.5

10W Heat Only

Time (min)	T1 AVG (C)	T2 AVG (C)	T3 AVG (C)	T4 AVG (C)
0	20.2	20.2	20.4	20.4
10	22.7	26.4	29.4	35
20	28.2	36	40.7	47.8
30	34.1	44.3	50.9	61.7
40	41.4	55.9	62.2	71.6
50	46.4	60.4	67.7	75.8
60	54.7	61.7	67.7	75.5
70	57.1	66	70.6	75.4
80	58.4	67.7	72.7	77.7
90	61	72.3	77.1	80.2
100	86.9	71	75.2	80.5
110	76.4	82.8	81.5	82.3
120	98.8	86.8	85.4	83.7

T5 AVG (C)	T6 AVG (C)	T7 AVG (C)
19.9	20	19.8
22.2	56	26.1
29	69.1	38
36.1	80.6	47.5
40.7	83.2	56.3
45.6	93.5	61.7
46.5	95.4	66.3
47.4	91	72.1
48.8	90.8	76.9
50.1	89.6	75.7
50.2	91.8	72.1
50.1	93	70.3
51.6	90.7	68.8

5W Heat + 4W US

Time (min)	T1 AVG (C)	T2 AVG (C)	T3 AVG (C)	T4 AVG (C)
0	20.3	20.2	20.3	20.3
10	21.2	23.1	24	26.7
20	24.8	32.4	35.9	41.6
30	30.5	41.5	46.5	54.5
40	36	49.2	56	66.8
50	39.9	54.3	61.4	70.3
60	45	60.2	67.2	75.6

T5 AVG (C)	T6 AVG (C)	T7 AVG (C)
20.2	20.2	20.2
31.3	25.6	24.1
41.9	50.7	34.4
55.2	61.2	44.2
64.8	68.8	51.4
65.7	74	56.4
69.1	79.4	61.1